# Chapter 6
# Size Effect in Physical and Other Properties of Nanostructured Coatings

## 6.1 Introduction

Rapid development of microelectronics in recent decades has been proven based on miniaturization and integration of electronic parts and according to the predictions of the ITRS[1] institute, this fast development will also continue in the next decade. In this regard, MOS field effect transistors or MOSFET[2] is the main and basic component of most of the electronic systems nowadays. Among the numerous parameters of these systems, MOSFET gate length, which is a critical criterion of integrated circuits, will decrease to about 10 nm in 2016 [1–6]. The predicted process of decrement of the gate length by ITRS, has been shown in the Figs. 6.1 and 6.2. The reasons for the dimensions decrease are as follow: improvement of the part's quality and performance, improvement of reliability, decreasing the power loss, improving the output efficiency, and decreasing its price.

Moreover, the speed of an electronic circuit is one of the most important factors. In order to increase the speed, parasitic capacity and serial resistances must be minimized so that RC delay time decreases and the Clock Frequency increase. Increment of the contact resistance in electronic parts has been one of the main limitations of size decrement in the recent decades. Hence, using new materials in joints has been considered in order to fix the circuit quality and increase the speed. In order to do so, metal silicides have been used in the process of metallization of joints and local systems. Selection of metal silicides has of great importance due to these reasons: their low special resistance, their contact resistances are low against both kinds of silicon, their high thermal stability, and their processes are compatible with silicon standard technology.

Nowadays metal silicides are an important component of an electronic part. The SALIIDE[3] process leads to the formation of a uniform type of metal silicides

[1] International Technology Roadmap for Semiconductors.

[2] Metal Oxide Semiconductor Field Effect Transistor.

[3] Self-aligned Silicide.

M. Aliofkhazraei, *Nanocoatings*, Engineering Materials,
DOI: 10.1007/978-3-642-17966-2_6, © Springer-Verlag Berlin Heidelberg 2011

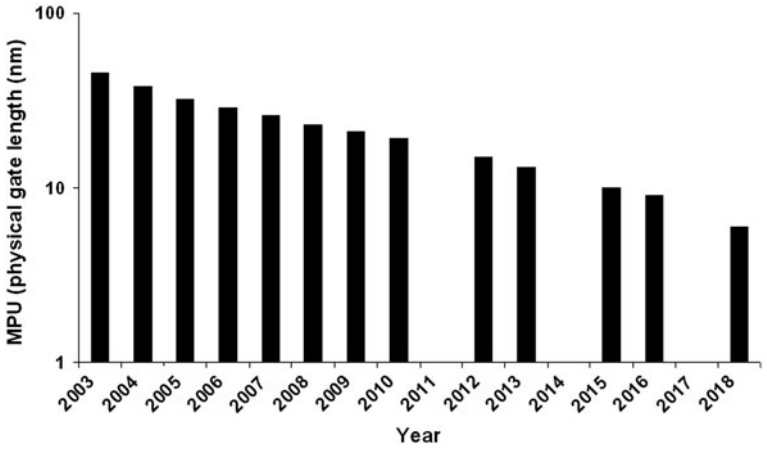


**Fig. 6.1** The approach of gate length decrease according to ITRS predictions

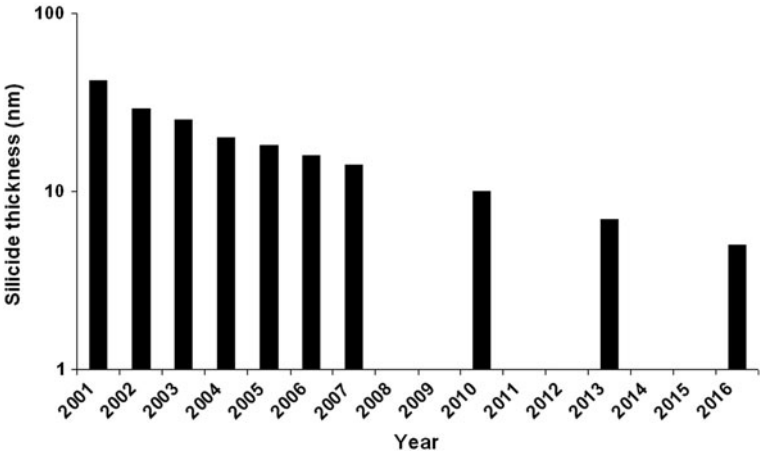


**Fig. 6.2** Approach to decrease the thickness of silicide in joints according to ITRS predictions

formed simultaneously in the regions of gate, source, and drain; and it is so successful due to its reliability and simplicity. Therefore, application of metal silicides has been promoted in electronics industry. The most common silicides used in electronic parts are PtSi, $TiSi_2$, and $CoSi_2$, although using C54–$TiSi_2$ (phase with less special resistance) and $CoSi_2$ in smaller parts (less than 0.2 and 0.04 μm respectively) is so difficult. In future parts we must use silicides layers with very low thickness. The silicides layer's thickness was about 20 nm in 2005, and it is expected that it will be reached to 5.5 nm in the year 2015 [7–14].

Recently NiSi has attracted much attention and the latest progresses reference to the vast efforts in order to the application of NiSi in MOS parts in future

technologies. NiSi is of great importance because of its low special resistance, low contact resistance, potential to form in low thicknesses, and its consistency. Therefore, it is inevitable to study its specifications.

Ohno et al. [15] described the control of the quantum size effect by controlling the coating layer thickness in $TiO_2$–$SiO_2$ core–shell hybrid particles obtained by the liquid phase deposition (LPD) method. The coating layer thickness of $TiO_2$ on $SiO_2$ nano-particles was controlled by changing the [Ti]/[Si] ratio. The titania coating thickness and crystallite size were estimated by transmission electron microscope (TEM) and X-ray diffraction (XRD), respectively. The quantum size effect of the obtained nano-hybrid particles was estimated by the band gap energy shift, using ultraviolet–visible spectroscopy (UV–vis). As a result, we successfully controlled the degree of the quantum size effect by controlling the coating layer thickness in core–shell $TiO_2$–$SiO_2$ hybrid particles.

The nano-particles have attracted considerable attention because of their potential application such as electronic, catalytic materials. The studies of nano hybrid particles have provided important fundamental insights for new functional materials such as photonic catalyst, high performance electronic materials and so on. Therefore, a lot of studies have been carried out to prepare the organic/inorganic hybrid particles. The quantum size effect has been widely studied for the microelectronic devices because of their recent trend of downsizing. In addition, several reports demonstrated that the quantum size effect resulted in the new properties and/or the improved properties. In general, the quantum size effect is expected for the nano-particles below 50 nm in many cases. However, there are difficulties in manipulation and handling of such nano-particles, mainly due to the agglomeration and the adhesion. Therefore, good handling method should be developed for the nano-materials with quantum size effect in many fields, such as electronics and so on. From this point of view, Ohno et al. [15] were proposed the nano-coating of functional materials on the nano-particles. They successfully prepared the $TiO_2$–$SiO_2$ hybrid particles by the modified sol–gel process. However, the obtained hybrid particles were not core–shell materials with homogeneous coating, and they couldn't control the quantum size effect. Therefore, they attempt to prepare the core–shell $TiO_2$–$SiO_2$ hybrid particles with homogeneous coating by LPD. LPD is well known as film deposition process, and some researchers applied the LPD method to prepare the $TiO_2$-Polystyrene (PS) Latex hybrid particles.

Ohno et al. [15] concluded the successful preparation of core–shell type $TiO_2$–$SiO_2$ hybrid particles by LPD. The coating layer thickness and the crystallite size were controlled by controlling the [Ti]/[Si]. In the case of the [Ti]/[Si] ratio of over 0.1, silica particles were completely coated by titania. The degree of the blue shift of the band gap energy by the quantum size effect for the obtained particles was approximately 0.13 eV larger than that of the pure titania, because of the existence of the Ti–O–Si bond. If the Ti–O–Si bond effect was removed, the blue shift of the band gap energy for core–shell type $TiO_2$–$SiO_2$ particles was nearly the same value as that of the reported values for the pure titania. From these results, the quantum size effect was successfully controlled by controlling the coating layer thickness of

core–shell type $TiO_2$–$SiO_2$ hybrid particles. Figure 6.3 illustrates the high resolution TEM (HR-TEM) image of surface morphology for the obtained $TiO_2$–$SiO_2$ hybrid particle with different [Ti]/[Si] ratio and the surface area of the obtained

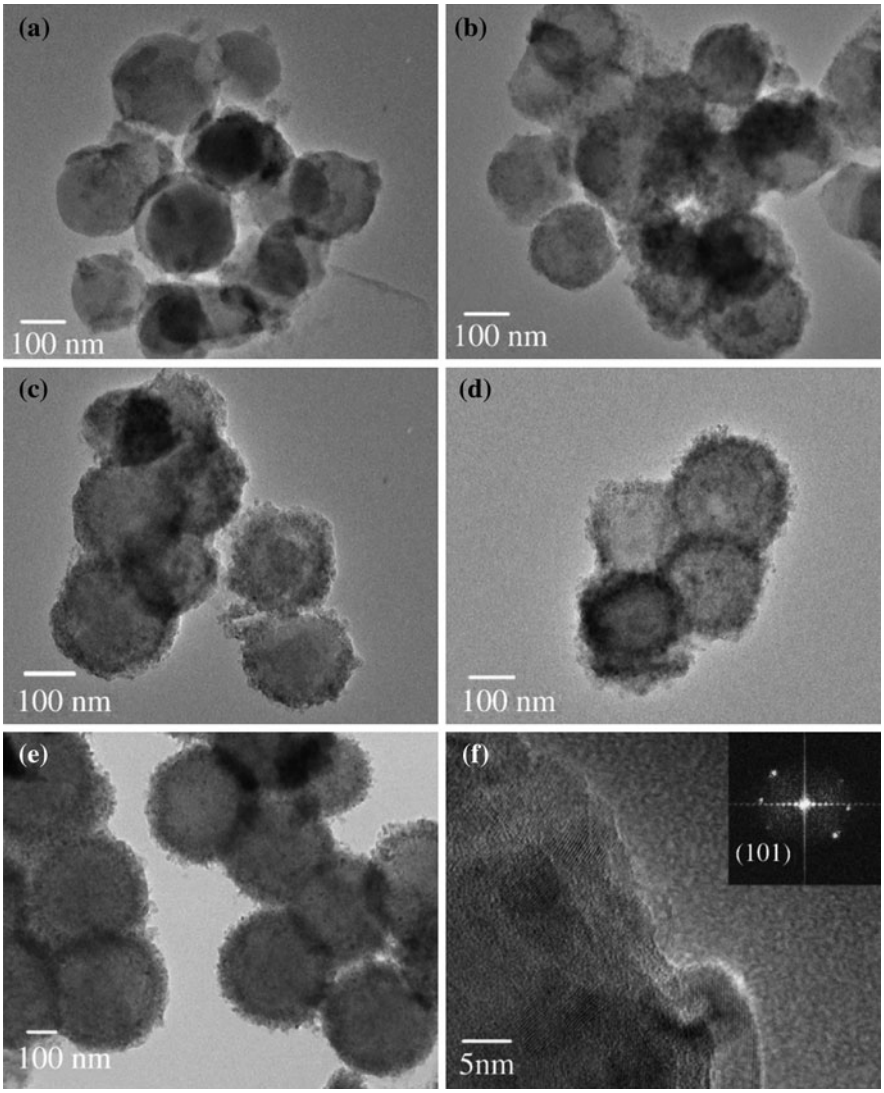


**Fig. 6.3** The surface morphology of the obtained $TiO_2$–$SiO_2$ hybrid particle with different [Ti]/[Si]: **a** [Ti]/[Si] = 0.1, **b** 0.3, **c** 0.5, **d** 0.75, **e** 1.0, and **f** high resolution TEM (HR-TEM) image of the surface area of the obtained hybrid particle with [Ti]/[Si] = 0.1, reprinted with kind permission from Ohno [15]

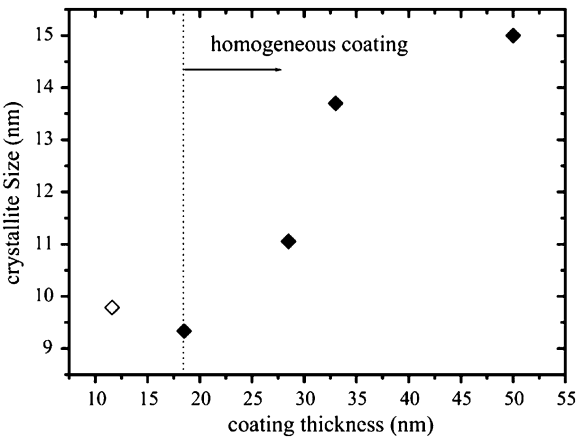


**Fig. 6.4** Change in the crystallite size as a function of the coating layer thickness, reprinted with kind permission from Ohno [15]

hybrid particle with [Ti]/[Si] = 0.1. Also Fig. 6.4 shows change in the crystallite size as a function of the coating layer thickness.

## 6.2 Silicides Specifications

Among different metal silicides, which are used in SALICIDE technology, $TiSi_2$ has been vastly studied due to its widespread application in CMOS[4] metallization. For the gate length 0.25 μm and for less than that $TiSi_2$ was replaced by $CoSi_2$. This substitution faces less resistance in low dimensions due to hard formation of C54–$TiSi_2$ phase [16–23].

### *6.2.1 SALICIDE Process*

SALICIDE process leads to the simultaneous formation of a uniform type of metal silicide in gate, source, and drain regions; and is of great importance in advanced electronic parts technology nowadays. SALICIDE process, for example, using the NiSi is described below. When gate is defined as a MOSFET, a Ni layer is layered on top of the sub-layer. The first thermal process, usually RTP,[5] at the low temperatures (often between 260 and 310°C) leads to the formation of $Ni_2Si$ in gate, source/drain areas where Si, which is in direct contact with layered Ni, is formed.

[4] Complementary Metal Oxide Semiconductor.

[5] Rapid Thermal Process.

No interaction happens between Ni and the surrounding oxide environment. After formation of $Ni_2Si$, the extra Ni layer is removed through selective wet etch method. The second thermal process usually forms NiSi in gate and source/drain areas between 450 and 500°C.

One of the advantages of Ni-SALICIDE is the application of single-stage thermal process (usually about 400–500°C). Practically, the problems related to non-uniform formation of NiSi and formation on Si lines with more thickness (thinner than wider lines) have made it necessary to use two-stage aniline process. SALICIDE process is applicable for Co and Ti, although the main objective of two-stage aniline process is different. The used temperatures for two-stage aniline depend on the type of silicide. In Ti and Co mode, the first aniline typically forms in thermal range of 650–700°C for C49–$TiSi_2$ and in 400–600°C for $Co_2Si$ or CaSo in order to prevent the formation of silicide on $SiO_2$ which causes a short circuit between the gate and source/drain electrodes. The second aniline is important to form low-resistance silicide phases C54–$TiSi_2$ (above 850°C) and $CoSi_2$ (above 700°C).

### *6.2.2 Necessary Conditions for Formation of Silicides*

Decreasing serial resistance and common parasitic resistances in gate, and source/drain areas is fundamental in order to improve the quality of the parts. Also, it is necessary that SALICIDE process do not influence the part and its alloying profile. The used metal in the formation of silicides must have the following basic conditions;

- high conductivity
- Low contact resistance for both alloyed Si types
- Good chemical stability in contact with Si
- Suitable mechanical and thermal specifications
- Suitable thermal stability considering the morphology
- Compatibility with standard processes technology of Si including Etching and Cleaning
- No need to extra thermal processes
- Void of harmful pollutions which decrease the efficiency of the part

Moreover, fundamental ideas to integrate the SALICIDE processes can be summarized in three ideas:

1. On the gate: formation of phase in low dimensions in thin lines of poly-silicon and small areas of single Si crystal in source/drain regions, morphologic and thermal stability of gate electrode-Silicide/Poly-Si.
2. On the source/drain: contact resistance between the silicide and source/drain and the integration of joint regions of source/drain.

3. Between the gate and source/drain: the bridge between gate and source/drain regions.

### 6.2.3 Transition from $TiSi_2$ to NiSi

Except the application of silicide as a barrier layer in contact with the common side of silicon and metal, Silicide was firstly used in LSI[6] as a poly-side (the electrode gate of poly silicon/silicide). The poly-side line $MoSi_2$ was one of the first applications of poly-side in DRAM[7] in early 1980. Then the poly-side $WSi_2$ was used for electrode gate of logic circuits LSI in mid 1980, due to its low resistance compared with $MoSi_2$. Application of $TiSi_2$ due to its low resistance compared with $WSi_2$ and its low contact resistance with both types of silicon, and also it's high thermal stability goes back to early 1990.

When the MOS parts' dimensions are minimized to 0.2 μm or less, the formation of $TiSi_2$ faces troubles. $TiSi_2$ has two structural phases: C49 and C54. The phase C54 is more sought to be used in these parts due to its lower special resistance and higher stability. The resistance of C49 has been reported between 60–80 μΩcm and that of C54 between 15–20 μΩcm. When the dimensions of the part decrease, the transition from C49 to C54 gets harder. The cause of this difficult transition is connected with low density of C54 nucleuses inside the C49 network. Since the transition of C49 phase to C54 is a process controlled by nuclear stage. On the Si lines, if the line thickness is less than the average distance between two nucleuses of C54, the formation of C54 phase will be dominated in single-manner development. This single-dimension development causes non-complete transformation of C49 to C54 and increases the resistance. Decreasing the dimensions of the part leads to the decrease of the temperature in which $TiSi_2$ starts to form. One of the ways to prevent this is to develop C54–$TiSi_2$ in thin lines, and also making the Si amorphous with the signal ion. In another different approach, the application of slow-fusible like Nb, Mo, Ta, and W has been suggested to form C54–$TiSi_2$.

The problems related to $TiSi_2$ in late 1990, led to the replacement of $TiSi_2$ by $CoSi_2$ in using lines thinner than 0.2 μm. $CoSi_2$ has a lower resistance compared to C54–$TiSi_2$. Regarding the technology based on Co, it seems that Co-SALICIDE has specifications like high formation temperature, oxygen impurities, high consumption of Si in forming silicide, formation of pores and inter-facial irregularities. High consumption of Si creates thick layers and creates problems in forming thin layers (less than 100 nm), so consumption of a suitable silicide free of all these problems will be necessary in manufacturing future parts.

---

[6] Large Scale Integration.

[7] Dynamic Random Access Memory.

### 6.2.4 NiSi Salicide Technology (Self-Aligned Nickel Silicide)

It is expected that NiSi is a good alternative for $TiSi_2$ and $CoSi_2$ in technologies which have 100 nm scale and smaller. In fact, NiSi has some fundamental advantages for CMOS processes including:

1. Formation of silicide layers in low temperatures
2. Little consumption of silicon
3. Void of undesirable bridging specifications
4. Little mechanical tensions
5. Having no effect of thin line on surface resistance
6. Low contact resistance to both types of Si (n and P)
7. Independence of resistance of silicide layer from decrease of thickness of connection lines

The formation of self-aligned silicide happens after the formation of source/drain. Therefore, the temperature formation of silicide must be low enough to keep the joint thin in under 100 nm CMOS technologies. NiSi has the lowest formation temperature among all the silicides, and the thermal stability interval is 350–750°C. For $TiSi_2$, the thermal stability interval is very limited. Contact resistance of $TiSi_2$ is high before 800°C, due to the presence of C49 crystal phase. Between 850°C and 950°C it decreases due to the formation of phase with formation of C54. Above the 950°C, due to the accumulation of surface resistance, it increases. In the other words, the contact resistance of NiSi gets stable and minimized between 350°C and 750°C. The increase of resistance above 750°C is due to the fusion of phase from NiSi to $NiSi_2$. Therefore, NiSi is thermally suitable for the technologies under 100 nm. In the other words, it must be kept in mind that the temperatures of processes after the formation of silicide must not exceed 750°C [24–37].

## 6.3 Size Effect in Sensing Characterization

Tan et al. [38] prepared non-equilibrium nanocrystalline $xSnO_2$-$(1-x)\alpha$-$Fe_2O_3$ powders by using the mechanical alloying technique. The thick film screen printing technology is then employed to fabricate these ethanol gas sensors. Their particle size and structural properties are systematically characterized using X-ray diffraction (XRD) and transmission electron microscopy (TEM). The gas sensing characteristics are also measured. Based on the experimental results, it was observed that particle size of the powders is drastically milled down to about 10 nm after 24 h of high-energy milling. A very high gas sensitivity value of 845 for 1000 ppm of ethanol gas in air has been obtained. New structural model for these non-equilibrium nanocrystalline $xSnO_2$-$(1-x)\alpha$-$Fe_2O_3$ materials explains both the lattice expansion of these high energy mechanically alloyed powders as

well as the charge neutrality in terms of additional oxygen dangling bonds at the nano-sized particle surfaces. It is those enormous oxygen-dangling bonds at the particle surfaces that give rise to the high gas sensitivity. The sensors are found to be 32.5 times more selective to the ethanol gas compared to CO and $H_2$ gases.

The increase concern over safety in civilian homes and industrial activities has generated great interest for reliable gas detection. Many thick film metal oxide semiconductor gas sensors based on their resistive changes, such as $SnO_2$ and $Fe_2O_3$, have been commercially designed to detect toxic gases (e.g., $CH_4$, CO, and $NO_2$). Nano-sized materials have been widely used to produce new semiconductor gas sensors, owing to the great surface activity provided by their enormous surface areas. Hence, they are expected to exhibit higher gas sensitivity. Being a promising gas sensing material, nano-sized $\alpha$-$Fe_2O_3$ powders have been prepared by various methods, including chemical co-precipitation, sol–gel process, metallo-organic deposition (MOD), and plasma enhanced chemical vapor deposition (PECVD). These methods are basically chemical processing techniques to build homogeneous structure on an extremely fine scale of a few nanometers from the molecular level. Tan et al. [38] used a different technique called the high-energy ball milling technique to obtain nano-sized $\alpha$-$Fe_2O_3$-based powders as the sensing materials. In this technique, the decrease of the particle size into fine powders of a few nanometers arises from the high-energy impacts during the collisions. This method, which is also known as mechanical alloying, has recently been used to prepare nano-sized $SnO_2$-($\alpha$-$Fe_2O_3$)-based powders with the grain size down to 8 nm for gas sensing. Such initially immiscible, mechanically alloyed $SnO_2$-($\alpha$-$Fe_2O_3$) materials are far from their equilibrium state. It is suggested that the content of $Sn^{4+}$ ions may play an important role in the gas sensitivity. However, the sensing mechanism in this $SnO_2$-($\alpha$-$Fe_2O_3$) system has not been well understood because of the lack of a complete understanding of the microstructure of the materials.

Tan et al. [38] have illustrated a promising method of using mechanical alloying in the preparation of nano-sized $\alpha$-$Fe_2O_3$ materials for gas sensing applications. In particular, the sensor has shown good ethanol gas sensitivity values of as high as 845 at 1000 ppm in air. The sensor is selective to ethanol gas

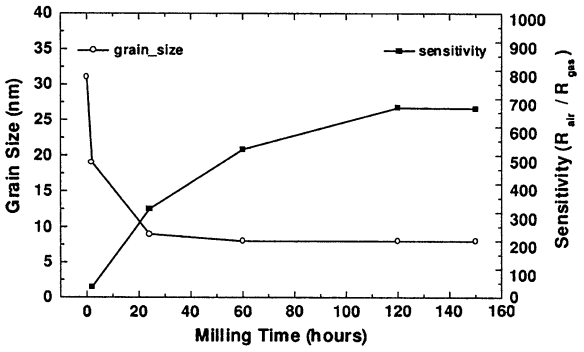


**Fig. 6.5** Correlation between grain size and sensitivity for different milling times, reprinted with kind permission from Tan [38]

over carbon monoxide and hydrogen gases. The gas sensitivity is also found to be very stable. These excellent experimental results can be explained by the fact that such mechanical alloying materials have nano-sized particle grains and exhibit enormous oxygen dangling bonds at their particle surfaces. Figure 6.5 shows correlation between grain size and sensitivity for different milling times while Fig. 6.6 illustrates TEM micrograph for powders after different milling times.

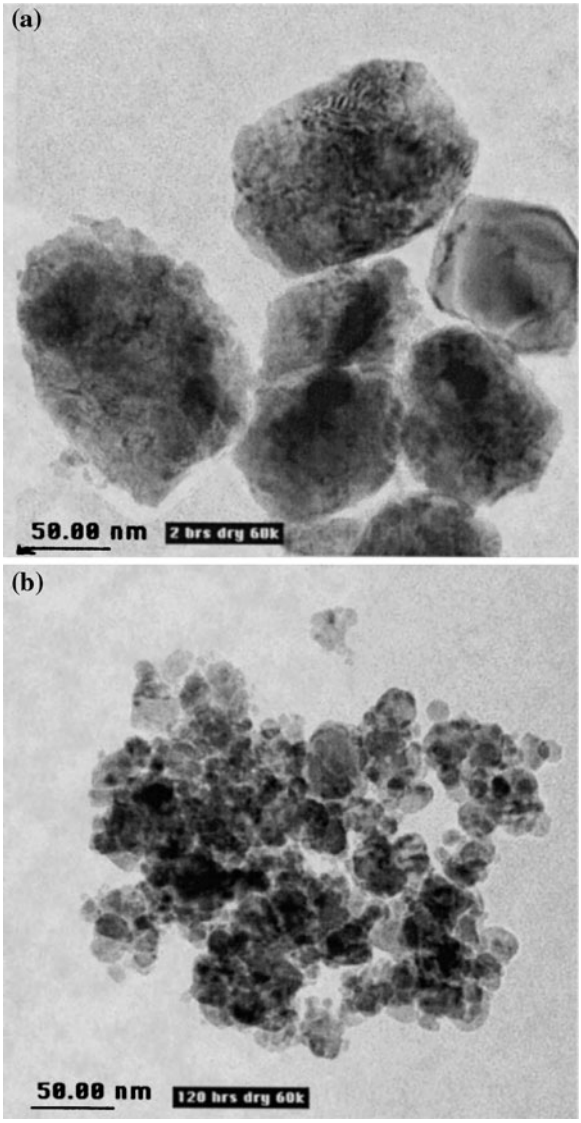


**Fig. 6.6** TEM micrograph for powders after (**a**) 2 h and (**b**) 120 h of milling, reprinted with kind permission from Tan [38]

## 6.4 NiSi Thermal Stability

### 6.4.1 NiSi Transition to $NiSi_2$ in Dual Ni-Si System

Thermodynamically, the formation of silicide is a result of decrement in reaction's free energy. When a metal is heated by contacting the silicon, and silicide is formed, the silicide phase is dependent on the formation temperature. In Ni-Si system (Fig. 6.7) and in the temperatures around 200°C, the $NiSi_2$ is formed, in temperatures around 350°C the NiSi is formed, and in temperatures around 750°C $NiSi_2$ is formed.

Contrary to the $Ni_2Si$ and NiSi situations, $NiSi_2$ development is non-uniform. Phase NiSi is stable to the temperature 750°C, NiSi reacts with the silicon sub-layer to form $NiSi_2$ which looks like the development of islands in NiSi network. An irregularity is seen in the common line of Silicide-Si. This irregularity is caused by the development of branches in some parts of the layer. The concentric development of the particles, reminds us of dendrite development inside the pillar particles. By time, more NiSi aniline is transformed into $NiSi_2$ and other $NiSi_2$ particles develop in order to reach each other. These big particles seem to be composed of smaller pillar particles. Numerous factors like temperature and the structural condition of previous phase seem effective in defining the new phase.

NiSi layer consists of particles with different crystal structures (cubic and orthorhombic). Adjacent particles are aligned optionally and cause the formation of some big particles. In temperature 700°C and after annealing, 5 min of swelling effect of each particle is seen under the silicon layer, which makes the common line of Si-Silicide have waves. This is direct effect of penetration of Ni network from NiSi into Si sub layer in the process of formation of $NiSi_2$. A large portion of Ni transfer is in the form of network penetration compared with penetration into the border of particles, and this can be due to the effects of swelling. The effects of swelling also depends on the structure, for instance for orthorhombic structure, the penetration ratio is low; therefore, the swelling ratio also decreases [24, 34, 35, 39–47].

### 6.4.2 Pt Effect in Increasing Thermal Stability

Pt and Ni have the same metallurgic behavior. In a crystallographic view, NiSi and PtSi have orthorhombic MnP structure, which is belonging to Pnma spatial group. Therefore, it can be expected that NiSi and PtSi are well solved in each other, and

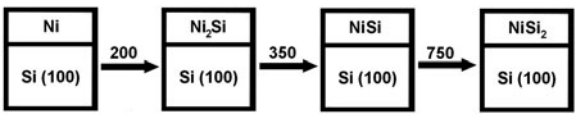


**Fig. 6.7** Stages of formation of different phases based on temperature (°C)

so increase $NiSi_2$ nucleus-formation temperature. Some researchers have studied the effect of little (about 5%) in thermal stability of NiSi layer on the surface of Si(111) and Si(100). XPS[8] and XRD[9] together show the increase of thermal stability until the temperature 850°C. The constant negative section of NiSi for the second sample has of high stability to 850°C. Moreover, by increasing the temperature, the difference between bonding energy decreases, which shows that Pt has a constant distribution in NiSi structure. This result is also confirmed by XRD spectrum and for the sample without platinum, $NiSi_2$ is formed in the temperature 750°C, but for other samples the formation of $NiSi_2$ is delayed until the temperature 900°C.

XRD spectrum shows some of the high-pressure textures for NiSi, which largely decreases energy for the common line of NiSi/Si compared with poly crystal NiSi layer without the Pt. As it was mentioned, PtSi and NiSi have the same structures. Therefore, Gibbs free energy NiSi, G(NiSi) is largely decreased due to the formation of NiSi(PtSi). On the other hand, Pt is not solved properly in $NiSi_2$, so it creates a little change in $G(NiSi_2)$. Hence, we can ascribe $NiSi_2$ nucleus thermal rise to the decrease of G(NiSi), and the rise of common line energy can be attributed to the trend to the formation of NiSi with high-pressure texture on the Si. In fact, the formation of $NiSi_2$ is done because of the following reaction.

$$Ni_{1-x}Pt_xSi + (1-x)Si \rightarrow (1-x)NiSi_2 + xPtSi \tag{6.1}$$

This shows that the presence of PtSi together with $NiSi_2$ will increase $\Delta\sigma$ in comparison with the normal reaction $NiSi + Si \rightarrow NiSi_2$. Besides, the formation of $Ni_{1-x}Pt_xSi$ largely decreases Gibbs energy:

$$\Delta_G(Ni_{1-x}Pt_xSi) = (1-x)_G(NiSi) + xG(P+Si) - T\Delta S_{mix} \tag{6.2}$$

Where:

$$\Delta S_{mix} = -R[x\ln x + (1-x)\ln(1-x)] \tag{6.3}$$

So the change in Gibbs energy for the relation (6.1) will be as:

$$\Delta G_1 = (1-x)[G(NiSi_2) - G(NiSi) - G(Si)] + T\Delta S_{mix} = (1-x)\Delta G_0 + T\Delta S_{min} \tag{6.4}$$

For $x = 0.05$, the $T\Delta S_{min}$ will be about 2 kg/mol in 1100 K, which is of the $\Delta G_0$ degree. Therefore, the driving force to transform the reaction $NiSi \rightarrow NiSi_2$ has decreased.

Some researchers studied the Pt inter-layer effect in stabilizing the NiSi layer on Si(111). The results show that by increasing the temperature, the direction of (200) NiSiII(111)Si will change into the direction (002) NiSi11(m)Si. Such a

[8] X-Ray Photoelectron Spectroscopy.

[9] X-Ray Diffraction.

transformation can not be seen in the previous work. The texture of NiSi layer from (200) NiSi11(111) into (002)NiSi11Si(111) will be transformed in high temperature after aniline. $NiSi_2$ nucleus will take place in NiSi texture after this transformation. This transition in the texture will consume some kinetic energy of atoms and the $NiSi_2$ nucleus configuration will be delayed. The comparison of surface resistance in two samples of Ni/Si and Ni/Pt/Si according to aniline temperature in the Fig. 6.8 confirms the previous discussions on the delay on formation of $NiSi_2$.

As mentioned before, by decreasing the dimensions of micro electronic parts, the thickness of joints will also decrease. For instance for a line thickness of 130 nm, the silicide layer will be about 34 nm. So, studying the thermal stability will have great importance by decreasing the thickness of metal layers signaled on Si and aniline. This has been studied by evaluating the following systems which have been annealed in different temperatures.

A. Ni (50 nm)/Pt(4 m)/Si(100)
B. Ni(25 nm)/Pt(2 nm)/Si(100)
C. Ni(12.5 nm)/Pt(nm)/Si(100)

Studying NiSi(211) peak situation in the temperature 800°C for one hundred samples shows that Pt percentage in all the samples is a fixed value, therefore the difference in transition from NiSi to $NiSi_2$ in samples; is not only related to the layers' thickness. The effect of thickness of the layer on thermal stability of NiSi in Ni/Pt/Si(100) system has been shown in Fig. 6.9. In the sample A in temperature 840°C, the surface resistance is increased from 1.7 to 2.3 $\frac{\Omega}{Sq}$. Considering the XRD results, the increase in surface resistance is due to the formation of $NiSi_2$. In the sample B, transition temperature happens at 80°C and in the sample C, it remains

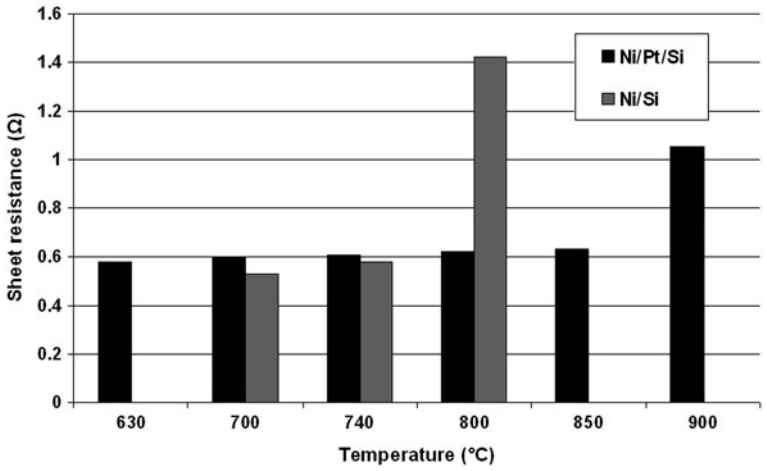


**Fig. 6.8** Changes of surface resistance according to baking temperature for Ni/Si and Ni/Pt/Si systems

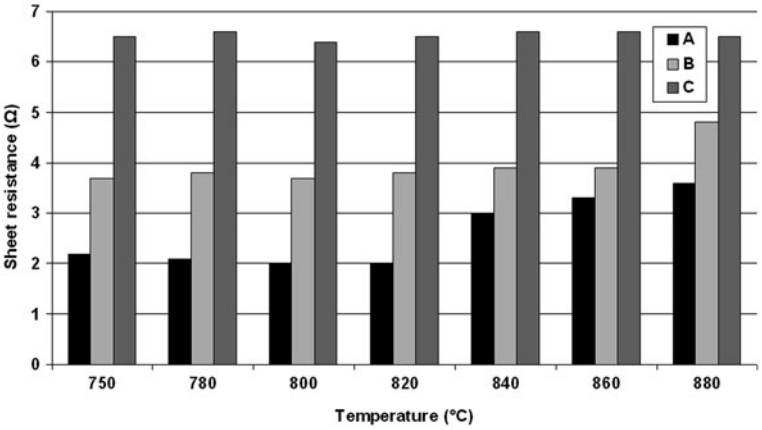


**Fig. 6.9** Surface resistance according to different baking temperatures

with the surface resistance even after 880°C. Therefore, we can understand that by decreasing the thickness in Ni/Pt/Si(100) system, thermal stability is increased. As we said before, the increase of platinum, decreases $|\Delta g|$ and this leads to increase of activation energy for nucleus. Also decrease of $|\Delta g|$ will ultimately increase the critical radius for the nucleus $r^*$.

As only the nucleuses with radiuses bigger than $r^*$ are allowed to develop, when the layer's thickness is low, the development will be limited in the direction of perpendicular with the layer's surface, and the nucleus will be delayed. We can have a numerical estimation from the value of $r^*$. For the normal reaction $NiSi + Si \rightarrow NiSi_2$, the quantity equals $-2.35\frac{kcal}{mol}$ or $-9.83\frac{kJ}{mol}$. Considering the structure (cubic, $CaF_2$) and constant network of $NiSi_2$ ($a = 5.4$ Å), Gibbs free energy in the unit of volume will be $\Delta_{g0} = -413\frac{J}{cm^2}$. Considering the critical radius:

$$r^* = \frac{2_b \Delta\sigma_i}{3_a |\Delta_{g0}|} \tag{6.5}$$

And also that $\Delta\sigma$, change in inter-layer energy is of $10^{-4}\frac{J}{cm^2}$ degree, the approximate value of $r^*$ for $NiSi_2$ will be about some nanometers.

### *6.4.3 Pd Effect in Thermal Stability*

Palladium, Pd, increases thermal stability of NiSi like Pt do. It is interesting to compare how Pd and Pt increase thermal stability. Some researchers have dealt with this issue by studying Ni/Pt/Si and Ni/Pd/Si systems. In their study, Ni's thickness has been chosen as 100 nm and Pt and Pd's were equally picked as 8 nm.

For the sample having Pt, a high pressure peak NiSi(200) exists and this means that there is a strong alignment in this structure. Such a texture is not seen in the sample having Pd. Aniline in temperature 900°C shows that in samples containing Pd, transition is done fully, but in samples with pt, NiSi(002) phase exists next to the formation of $NiSi_2$, which prevents the completion of the transition. That is in presence of Pt, the system shows more stability. These results are compatible with the results produced by Raman analysis.

Pt and Pb both increase nucleus activation energy $NiSi_2$, because PdSi and PtSi have a similar structure with NiSi and form a solid solution. But this increase is more for Pt, and it is because of justification direction NiSi(200)11Si(111). This direction decreases inter-layer energy between NiSi and Si(111) which rises $\Delta\sigma$ and $\Delta G^*$, so that we have:

$$\Delta G^*(\mathrm{Ni/Pt/Si}) > \Delta G^*(\mathrm{Ni/Pd/Si}) > \Delta G^*(\mathrm{Ni/Si}) \tag{6.6}$$

Comparison of thermal stability of these three systems is there in Table 6.1 with considering inter-layer energy effect $\sigma$ between NiSi and Si, and the driving force $|\Delta G|$ for nucleus configuration. Increasing the inter-layer thickness Pd will increase the system's thermal stability. For example, with Pd thicker, it shows more stability and when the thickness increases to 7 and 10 nm, nucleus configuration of $NiSi_2$ will be delayed until 900°C.

### 6.4.4 Ge Effect in Thermal Stability

Ge also increases temperature in nucleus configuration $NiSi_2$. For system Ni/Ge/Si the phase transition from NiSi to $NiSi_2$, even at 900°C will not complete in comparison with NiSi (800°C), and it proves a considerable rise in nucleus configuration of $NiSi_2$. A layer's conductivity also depends on its morphology, since after aniline at 800°C, the NiSi layer is developed on Ge/Si evenly, and it gets irregular and uneven by increasing temperature. The accumulation of atoms takes place by forming $NiSi_2$. The temperature for nucleus configuration in the reaction of layer Ni with sub layer $Si_{1-x}Ge_x$ increases too. In both cases, we could attribute temperature rise to the entropy effect of NiSi–NiGe mixture. NiGe has a Mnp structure, similar to that of NiSi, and so Ge is well solved in NiSi but not in $NiSi_2$. So, the level of free energy decreases as $T\Delta S_{\min}$ and the pure value decreases, consequently activation energy $\Delta G^*$ related to $NiSi_2$ nucleus configuration also increases.

**Table 6.1** Comparison of thermal stability of NiSi with Pt and Pd barriers

| | $\sigma$ decrease | $\lvert\Delta G\rvert$ decrease | Thermal stability sequence |
|---|---|---|---|
| Ni/Pt/Si(111) | Yes | Yes | 1 |
| Ni/Pd/Si(111) | No | Yes | 2 |
| Ni/Si(111) | No | No | 3 |

### 6.4.5 Co and Ir Effects in Thermal Stability

Some researchers have shown that using Ir and Co as penetration barriers, not only improves thermal stability, but considerably decreases leaking flow in thin joints with depth of 40 nm. In Ni/Si, the development of $NiSi_2$ plates in the direction (111) will increase surface resistance and leaking flow. The rise in stability and little leak of the flow is probably due to the very even common line in samples containing Ir and Co.

### 6.4.6 Capsulation and NiSi Thermal Stability

The contaminations caused by oxygen during silicide process might be resulted from following sources: (1) aniline environment, (2) Oxygen accumulated during metal's layer signaling (3) inter-layer oxide in silicon/metal common line. Inter-layer silicon oxide in the common line of Ni/Si decreases the reaction between Ni and Si too. So taking methods to absorb oxygen from Si surface is necessary. Ti Capsulation also decreases the inter-layer oxides. Also the Ti cap increases regularity and thermal stability, and also decreases the leak in flow. Before annealing, Ti surface is covered with a $TiO_2$ oxide layer. During aniline at 500°C, two important things happen: First, Ti cap has more reaction with oxygen. Second, Ti atoms in cap penetrate into Ni layer, and accumulate in the common line of Ni/Si. Aniline at 600°C not only forms NiSi, but also forms Ti–Ni–Si (TiNiSi and $(TiNi_x)Si_y$) and a layer of $TiOSi_2$. The formation of NiSi at 600°C shows the restoration of $SiO_2$ by Ti.

$SiO_2$ cap layer also delays the surface resistance. For the capped samples, the surfaces get more irregular with increasing temperature. The arrows show areas not covered by silicide. The density of these areas is more for capped samples. Using the cap layer also forms an even layer of silicide. Using the cap also decreases the development of furrows, and the morphologic behavior of NiSi layers' surface, in cap case or without the cap, are bound with the furrows. In the other words, using cap layer delays the appearance of thermal furrows and so the accumulation of NiSi atoms, that is decreases the cap layer of surface energy NiSi.

Finally, one of the most important challenges in miniaturizing the parts in electronic industry that is, increasing the resistance when the dimensions decrease was studied here. By decreasing the thickness, the resistance increase in joints. We also mentioned some specifications and capabilities in using $TiSi_2$ (phase C54) and $CoSi_2$. $TiSi_2$ has two structural phases of C49 (high resistance) and phase C54 (low resistance). By decreasing the thickness of lines in joints; transition from high resistance phase to low resistance phase becomes more difficult. Therefore, using $TiSi_2$ for dimensions lower than 200 nm faces the problem of resistance rise. $CoSi_2$ as an alternative for $TiSi_2$ has some basic problems despite the low resistance, including high consumption of silicon and high formation temperature

(550°C). High consumption of silicon makes it more difficult to develop this layer in nanometer dimensions. Silicide Nickel (NiSi) with low special resistance, even in dimensions lower than 100 nm, and with less silicon consumption, lower formation temperature (350°C), etc. can be a good replacement for $TiSi_2$ and $CoSi_2$.

The only problem relating the limited thermal stability is due to the fusion into a phase with the resistance more than $NiSi_2$ at 750°C, and the taking place of Agglomeration phenomenon on the surface. We mentioned some of the studies by researchers in recent years, like using different types of impurities or taking penetration barriers to improve thermal stability of NiSi, and we studied the reasons for thermal stability rise in the framework of classic theory of nucleus configuration and the effect of entropy mixture [48–57].

## 6.5 Size Effect in Optical Properties of Nanostructured Films

Kale et al. [58] fabricated cadmium selenide nano-crystallites onto amorphous glass substrate from an aqueous alkaline medium, using chemical bath deposition method at room temperature. The samples are annealed in air for 4 h at various temperatures and characterized by structural, optical and electrical properties. The as-deposited CdSe layers grew in the nanocrystalline cubic phase, with optical band gap, '$E_g$' 2.3 eV and electrical resistivity of the order of 106 Ω cm. After annealing metastable nanocrystalline cubic phase transformed into stable polycrystalline hexagonal phase. Depending upon temperature, decease up to 0.6 eV and 103 Ω cm were observed in the $E_g$, and electrical resistivity, respectively. These changes have been attributed to the increase in the grain size of the CdSe crystallites.

Presently nanocrystalline materials have opened new chapter in the field of electronic applications, since material properties could be changed by changing the crystallite size and/or thickness of the film. New applications in various fields are also emerging. Development of such materials, whose structural, electrical and optical properties could be controlled, will be useful many ways. For example optoelectronic devices, particularly solar energy conversion devices could be modified accordingly.

The synthesis of binary metal chalcogenide of groups II–VI semiconductors in a nanocrystalline form has been a rapidly growing area of research due to their important non-linear optical properties, luminescent properties, quantum-size effect and other important physical and chemical properties. The semiconductor nanocrystallites belong to state of matter in the transition region between molecules and solids. Their physical and chemical properties are found to be strongly size dependent. The properties of materials prepared by different methods are critically dependent on the nature of preparation technique and subsequent heat treatments like annealing in air, vacuum or different gaseous environments like $H_2$, $N_2$, Ar, etc. The micro-structural features of nanocrystallites are found to govern their electro-optical behavior. Cadmium selenide ($E_g = 1.7$ eV) is one of the

promising semi-conducting material that has been studied for application in solar cells, $\gamma$ ray detectors, thin film transistors, etc. A number of workers have chemically prepared CdSe thin films. However, little attention has been paid to the various properties of chemically deposited CdSe thin films.

Kale et al. [58] report on the room temperature chemical deposition of CdSe thin films from an aqueous alkaline medium. In order to get good quality CdSe thin films, the preparative parameters such as concentration of cadmium, deposition time and pH were optimized. Freshly deposited thin films may contain many defects such as voids, pinholes, etc. Annealing of thin films reduces the defects and increases crystallite size along with recrystallization process. Kale et al. [58] deposited the CdSe thin films by aqueous alkaline medium at room temperature grows with nanocrystalline phase with band gap 2.3 eV and electrical resistivity of the order of 106 Ω cm. Air annealing was found to increase crystallinity of the CdSe films along with recrystallization process that changed nanocrystalline to metastable cubic to stable hexagonal phase (673 K) at higher annealing temperature. The crystallite size of the particles was increases as a result of increasing the annealing temperature. Consequently, the electrical resistivity was decreased and CdSe films showed 'red shift' of 0.6 eV. Figure 6.10 shows plot of CdSe crystallite size versus annealing temperature of CdSe thin films. Tabulation of crystallite size, band gap '$E_g$', electrical resistivity and activation energy of as-deposited and annealed CdSe thin films can be seen in Table 6.2.

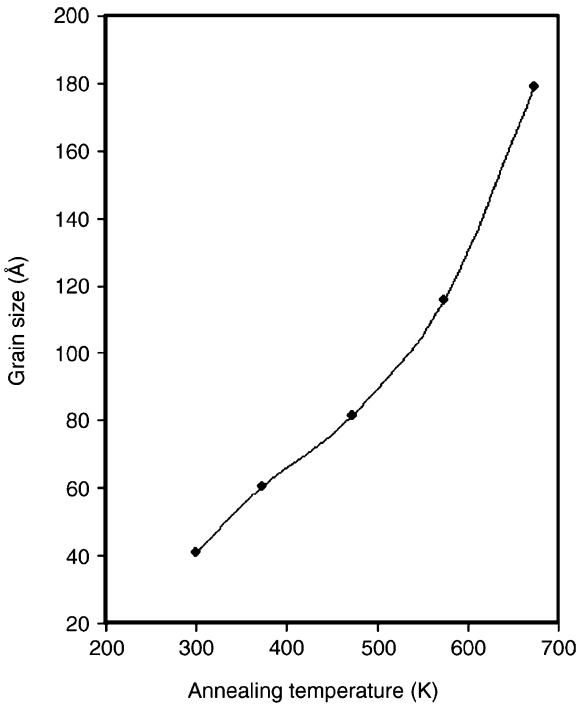


**Fig. 6.10** Plot of CdSe crystallite size versus annealing temperature of CdSe thin films, reprinted with kind permission from Lokhande [58]

**Table 6.2** Tabulation of crystallite size, band gap '$E_g$', electrical resistivity and activation energy of as-deposited and annealed CdSe thin films, reprinted with kind permission from Lokhande [58]

| Thin films | Crystallite size (Å) | Band gap '$E_g$' (eV) | Electrical resistivity (Ω.cm) | Activation energy (eV) | |
|---|---|---|---|---|---|
| | | | | HR | LR |
| As-deposited | 40 | 2.3 | $3.25 \times 10^5$ | 0.86 | 0.34 |
| 373°K | 60 | 2.0 | $9.58 \times 10^4$ | 0.79 | 0.31 |
| 473°K | 80 | 1.8 | $5.38 \times 10^4$ | 0.72 | 0.27 |
| 573°K | 120 | 1.8 | $8.23 \times 10^3$ | 0.69 | 0.18 |
| 673°K | 180 | 1.7 | $1.17 \times 10^3$ | 0.65 | 0.16 |

*HR* high temperature region and *LR* low temperature region

Du et al. [59] prepared nano-copper films by DC magnetron sputtering. Their reflectivity and transmittivity to electromagnetic wave in infrared region were measured with Fourier Transformation Infrared Spectrometer (FTIR), by which their complex optical constant and permittivity were obtained. The results show that the complex optical constant and permittivity of nano-copper films depend upon the film thickness. This dependence is correlated with microstructure transition during the film growth.

Nano-sized metal films have been of considerable interest both from fundamental point of view and for potential applications in photonics and electronics devices based on their unique properties which are generally very different from bulk materials. For example, it has been shown that electrical conductivity, $\sigma$, of ultrathin metal film decreases apparently with its decreasing thickness. Strong interaction between metal films and electromagnetic wave occurs when the film thickness decreases to nanometer scale. Meanwhile, electromagnetic compatibility (EMC) of overall quality of nanostructured materials, devices and systems becomes a more and more serious question with decreasing size and increasing working frequency of electronic systems. In those cases, a precise knowledge on the complex optical constant and complex permittivity of ultra-thin metal films, for a thickness range from a few nanometers up to opaque layer, is very important.

Copper as a kind of metal with high conductivity, electromagnetic performances of its films have been widely studied for the application in Integrated Circuit (IC) and microelectronics devices as interconnection parts, in semimirrors as UV radiation filters and as telescope mirror layers. Du et al. [59] deposited nano-copper films by magnetron sputtering method. Since the complex optical constant and the complex permittivity are not directly measurable quantities, they are calculated with reflectivity and transmittivity of copper films to electromagnetic wave. At the same time, the thickness dependence of nano-copper films on complex optical constant and permittivity are analyzed.

Du et al. [59] measured the reflectivity and transmittivity of nano-copper films to electromagnetic wave in infrared region, by which their complex optical constant and permittivity, both the real and the imaginary parts are calculated. All these parameters are essentially dependent on the film thickness. This dependence

should be considered in application of nano-copper film. The dependence of electromagnetic parameters on the characteristic size provides new possibilities for designing high performance electromagnetic functional materials and devices. The evolution of the film microstructure plays an important role in the size effect of nano-copper film on complex permittivity. Figure 6.11 shows dependence of reflectivity (a), transmittivity (b) of nano-copper films on thickness in infrared region. Figure 6.12 also shows dependence of complex optical constant real and imaginary parts of nano-copper films on thickness in infrared region.

Tang et al. [60] reviewed studies on ultraviolet stimulated emission and lasing observed at room temperature from nano-structured ZnO thin films. The nano-structured ZnO thin films were grown on sapphire substrates using Laser-Molecular-Beam-Epitaxy (L-MBE). The thin film was consisted of regularly arrayed hexagonal nano-crystallite columns, whose facets form natural micro-cavities. These nano-crystallites confine the centre-of-mass motion of excitons. As a result of the quantum size effect, the oscillation strength of the excitons is largely

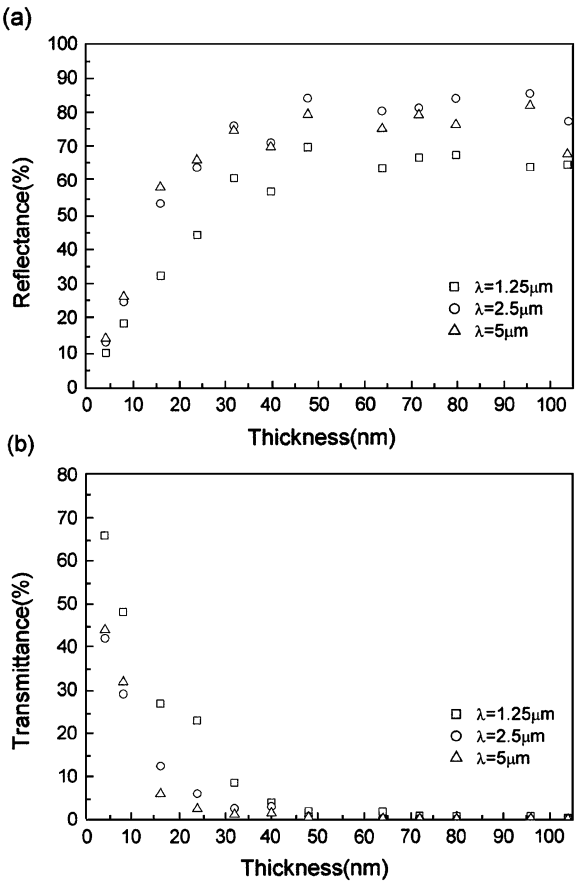


**Fig. 6.11** Dependence of reflectivity (**a**), transmittivity (**b**) of nano-copper films on thickness in infrared region, reprinted with kind permission from Du [59]

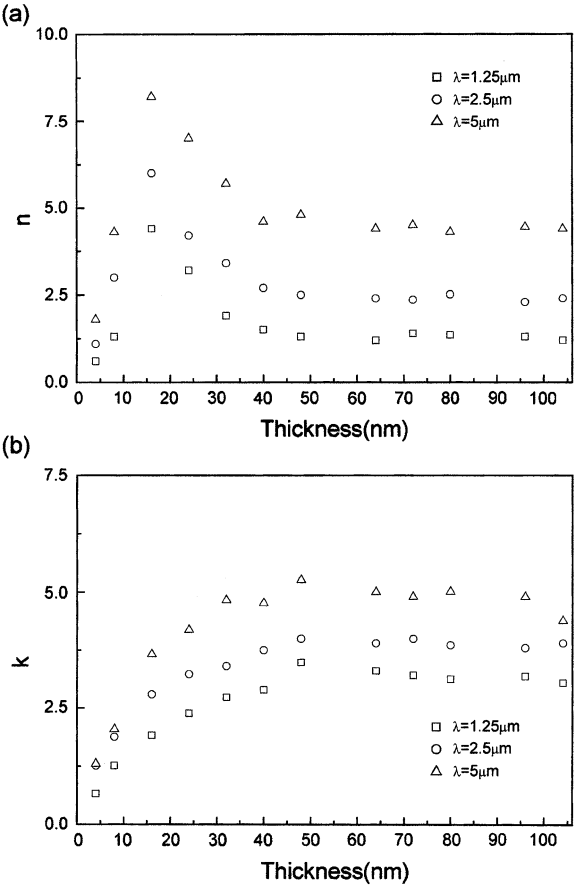


**Fig. 6.12** Dependence of complex optical constant real part (**a**), imaginary part (**b**) of nano-copper films on thickness in infrared region, reprinted with kind permission from Du [59]

enhanced, which is favored to the radiate recombination of exciton at room temperature. Excited using the frequency-tripled output of a YAG laser, the nanostructured ZnO thin film showed strong ultraviolet lasing at room temperature with a threshold as low as 24 kW/cm$^2$. At a moderate pumping intensity, the room temperature stimulated emission is associated with an exciton-exciton collision process. At higher pumping density, the excitons are dissociated, and the ultraviolet stimulated emission is dominated by an electron–hole plasma recombination process. Because of the large enhancement of oscillator strength of the excitons, the optical gain of the stimulated emission measured at room temperature reaches as high as 320 cm$^{-1}$, which is an order higher than that observed in bulk ZnO crystals. In comparison with the electron–hole plasma stimulated emission in most of commercial semiconductor lasers, the excitonic stimulated emission can be realized at relatively low external pumping density. The observation of excitonic lasing effect at room temperature might be valuable in realization of practical ultraviolet semiconductor laser devices.

Compact short-wavelength semiconductor laser diodes (SLDs) present vast possibilities in many high-technology applications. For example, in the area of optical storage, the storage density is limited by the size of the diffraction spot which is proportional to the square of the laser wavelength. Hence, the availability of short-wavelength SLD means much greater density of data can be stored on a disc. Towards this end, InGaAlP-based yellow SLDs had been developed with wavelength as short as 650 nm. Since this achievement, there was no report of shorter wavelength SLDs until 1990, when the first demonstration of green–blue lasing actions in ZnSe-based heterostructures was reported, followed soon by the successful operation of ZnSe-based laser diode in 1991. However, practical short-wavelength SLDs are still not available because the lifetime problem. Recently, room temperature (RT) ultraviolet (UV) stimulated emissions and laser emissions have been reported in metal nitride systems as a result of the breakthrough in the growth of high-quality GaN-based heterostructures and successful development of p-type doping.

ZnO, as an oxide, is superior over nitrides and selenides in thermal stability as well as in resistance to chemical attack and oxidation. Its RT band gap is 3.37 eV which is suitable for fabricating UV optoelectronic devices. Its large exciton binding energy (60 meV) should in principle favour efficient RT excitonic emission. Because of the current difficulty in heavy p-type doping, research works have been carried out for study on the properties of stimulated emissions using electron beam pumping and optical pumping for bulk ZnO crystal at cryogenic temperatures. Few works have been reported on the UV stimulated emission at room temperature in bulk ZnO crystal, but no emission spectra were given.

Tang et al. [60] reviewed their progress on ZnO nano-crystal ultraviolet laser research. The nano-crystallite thin films grown by the laser molecular beam epitaxy (L-MBE) consist of self-assembled, ordered arrays of hexagonal nano-crystallites. They described the structure and formation mechanism of the hexagonally shaped nano-crystals. The facets of the close-packed and ordered hexagonal nanocrystallites form natural lasing cavities. The optical gain is shown to be of excitonic nature and has a very large value that is dependent on the size of the nano-crystallites. The peak gain value is as high as 320 $cm^{-1}$ for a 55 nm thick film, an order of magnitude larger than the largest known value for bulk ZnO. The large gain is attributed to the modification of the spontaneous emission created by the dielectric photonic structure of these films. The observations reported demonstrated that ZnO may be a viable material for short-wavelength optoelectronics application. Figure 6.13 shows lasing threshold as a function of film thickness.

Bilotsky et al. [61] studied the size dependence of electron-lattice energy exchange in nanoparticles. Both surface and bulk energy exchange parameters are examined and it is demonstrated that the bulk energy exchange has non-monotonic oscillations versus size of the particles. It has been found that the amplitude of such oscillations increases with decreasing a particle size until the critical size reaches $L_c$. These bulk interaction related oscillations disappear for the particles less than $L_c$, and only the surface energy exchange remains as the energy flow

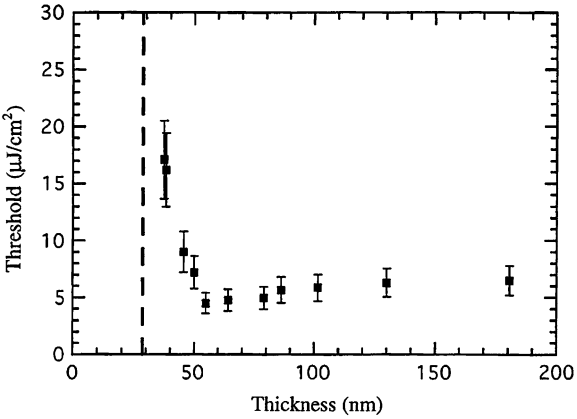


**Fig. 6.13** Lasing threshold as a function of film thickness. An excitation with a size of 500 μm × 30 μm stripe was used, reprinted with kind permission from Tang [60]

between electrons and phonons subsystems. It has been shown that there exists an interval of particles sizes with total energy exchange of few orders less than in massive bulk metals. This condition is crucial for existence of hot electrons in stationary conditions in metal nanoparticles, metal island films and thin films as have been observed experimentally.

Hot electrons in metal nanoparticles have been discovered experimentally, or more specifically, the lighting of gold nano-islands film on a dielectric was observed when a BIAS voltage was applied to the film. Electrical current flow resulted radiated light along the system of tunnel-connected island metal films (IMF). Later a new phenomenon has been observed—electron emission and non-linear current–voltage characteristics in IMFs altogether with lighting. These observations were made with applied voltage bias of $\sim$10–30 V but the application of the same voltage to continuous (thick) films or bulk metallic samples did not produce above-mentioned phenomena.

These phenomena were explained by a hot electrons concept. It should be noticed that hot electrons were observed in stationary condition in IMFs gold samples only but they did not appear in continuous films or bulk metal. However, hot electrons can be also obtained in IMFs by irradiation of a laser beam. Particularly, the irradiation with a pulsed $CO_2$ laser ($\tau \sim$ 0.2–1.0 μs) has been used. The duration of the pulse is much larger than all relaxation processes times in IMFs. The same phenomena (such as lighting and electrons emission in voltage applied experiments) have been observed in laser irradiation experiments. Therefore, the hot electrons appeared in quasi-stationary conditions in these experiments as well.

Bilotsky et al. [61] studied the total electron–phonon energy exchange in small metal particles which size is less than free path of electron–phonon collisions. This expression contains bulk and surface terms. The bulk contribution oscillates as the function of the particle size. It is important that the long wave acoustics phonons generated by the hot electrons can be in non-equilibrium state with others phonons. Thus, the use of electron–phonon collisions integral

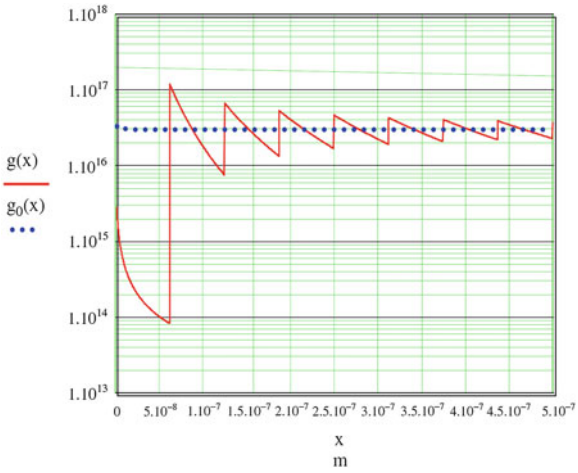


**Fig. 6.14** Electron-phonon energy exchange constants $g(x)$, $g_0(x)$ versus $x$, reprinted with kind permission from Bilotsky [61]

approach with Plank distribution function of phonons could be incorrect. As it has been mentioned above, the hot electrons have been observed in stationary conditions only in IMFs. Nevertheless, there is one common electron–phonon energy exchange feature for both IMFs and thin metal films. Microelectronic devices electric conductivity with such as thin conductors may be quite sensitive to a film thickness. Figure 6.14 shows electron–phonon energy exchange constants $g(x)$, $g_0(x)$ versus $x$.

## 6.6 Optical Coatings: Using Ultraviolet Light Block Layers

For a long time, removing and destruction of different substructures and substrates, such as polymer wooden sub-layers under ultraviolet light, was an important problem for construction and application of these pieces in different poor climates. During recent years researchers were able to solve this problem using nano-materials, particularly ones for nano-coating. It the past different materials were used, which did not enjoy decent quality and had defects during efficient absorption of ultraviolet light. Among disadvantages of traditional methods one can mention decrease of substance transparency and deactivation of ultraviolet resistant coating before end of piece life.

Through new method, nano-coating of surface is performed with pure and impure $ZnO_2$ and CuO nano-particles. Nanodur is one of important companies at this field. Using new coating leads to sufficient absorption of ultraviolet light. Compared with traditional ones, these coatings are of longer lifetime. Other advantages of these coatings are their higher resistance against cracking and abrasion, apparent transparency, and lack of deformation and color change. One of most important advantages of anti-ultraviolet nano-coating it their permanent

activity, in contrary with organic materials which deactivate after a while. These coatings can be applied to optimize most of pieces [62–74].

## 6.7 Surface Improvement for Making Fog and Vapor Resistant Layers

Researchers succeed to produce a fog and vapor resistant nano-metric surface through improving plastic and poly-carbonate surfaces. At this method a new formulation (Clarity Fog Eliminator) was applied to prevent development of fog and vapor on surface. These products can be used in lightproof, face protector, and common or sport eyeglasses. As well as mentioned applications, this product is even applicable in refrigerator environments.

## 6.8 Production of Pieces with Nano-Coating

Nanofilm Company is to produce products which use nano-coating technology. In most of these products coated part serves as main piece part and is considered among most important applications of nano-coating. One of applied coatings is one which repels water, snow, ice and other similar pollutions from the glass's surface. It is expected to use these glasses in automobile industry. Among other applications of these coatings one can name other cases such as eyeglasses. Another fabricated coating is steam resistant nano-coating for sport and military utilities, optical pieces, and customary, safety, and laser glasses. These pieces can be applied in car windscreen, bath mirrors, and etc. Another type of fabricated nano-coat is anti-reflection one, which can be appropriately used in interior mirror of cars and cosmetic cases. The coat prevents glaring reflection of the light.

## 6.9 Self-Cleaning Glasses

Self-cleaning glasses is addressed to glasses with photo-catalyst metallic oxide (especially titanium oxide) coatings, which its surfaces have hydrophobic properties. Due to sunlight or any source of ultraviolet light on activated surfaces these nano-coatings get activated and develop catalyst properties. Because of oxidizing feature of glass surface coating, any artifact is broken on the surface and converted to inorganic aqua-soluble material. Raining or water spraying on surface destructs surface of contaminator particles and causes to their collapse, for their hydrophobic property [75–84].

## 6.10 Medical and Hygienic Applications

### *6.10.1 Inorganic Materials Nano-Coating for Medical Applications*

Chemists at UCLA University have invented a new unique nano-coating for inorganic materials, which is capable to produce them similar to proteins. Using this method one can apply these particles as a measuring tool for detecting intercellular activities. Using these products can be followed by significant achievements in pharmacy and detecting tools. During this method nano-metric coating particles and quantum wires by fiber amino-acids with short loops (peptides) are used. Through this kind of coating living cell authorize entering and exiting of particles, due to their similarity with proteins. These inorganic materials can even be poisonous. The method makes it possible to perform some investigations in living cells at molecular scale, so this is one of most important applications of nano-technology in biology and medicine.

The method enables us to produce nano-coating on the surface of semi-conductor particles and import them as electronic measuring tools. Among their important applications one can name their fluorescence light reflection. During this method different particles can be imported to the living cells and be stimulated by blue light. Any of these particles have their own particular fluorescence response. Using different proteins coating with different fluorescence colors on nano-particles make it possible to use them as biological label. Researchers mention peptide nano-coating method as a link between organic and inorganic materials. Also, they consider their application as a method to produce intelligent drugs.

### *6.10.2 Using Nano-Particle Masks*

After onset of SARS, using anti-bacterium masks was of a great interest. Hence, efforts for fabrication of bacterium and tiny particles filter have been accelerated. One of interested fields of this part is nano-coating. Traditional coatings are able to stop bacterium to enter in living cells; in the other word the entrap bacteria on their coating. However, due to bacteria and other dangerous particles accumulation in masks they should be replaced as often as possible. To deal with this problem, using nano-coating was of a great interest among researchers. In these filters $TiO_2$ nano-particles coating or polluted nano-particles of silver are used. The main advantage of these filters is that they eliminate dangerous bacteria and organic particles; then applied filter has no need to be replaced and can be used for a long time. Applying such filters has been focused to prevent bacterium and virus entrance. As a considerable share of these materials fabrication leads to using nano-coating with nano-materials, there predicted to be a satisfactory market.

### 6.10.3 Application of Hydroxyapatite Nano-Coating to Design Prosthesis

IMC (Infromat Company) produces some prosthesis with nano-structured n-Hydroxyapatite HA coatings which serve as marker layer with electrophoretic method at common temperatures. In comparison with conventional pieces, newly made ones are of more compatibility with human body and are much cheaper. Coating according mentioned method and through nano-structures, compared with common coating methods, is of so many advantages such as enhancement of pieces strength, bonds stability, and resistance against corrosion. To examine features of this kind of coating there have been performed various tests to assess hardness of these pieces. One of these tests was for evaluation of coated Ti6Al4V pieces hardness, which reveals up to 3 times increase in cohesion and strength of surface coating. That mentioned coating is very dense and hard and exhibits a high resistance against corrosion in human body.

One of existed problems at this method is lack of adjustment thermal for expansion coefficient of titanium/HAP. This inequality against thermal expansion coefficient leads to development of stresses in the piece. Another existed problem during application of these pieces is development of an oxide, with low resistance against corrosion, at interface of titanium and nano-structure coating.

To solve the problem, IMC has used a glass coating, compatible with human body. Using this coating at interface of nano-structured coating and titanium the problem of incompatibility of thermal expansion coefficient can be easily removed. Besides, using similar coatings it is possible to prevent development of instable oxide at the interface.

Using nono-structural coating of nano-hydroxyapatite lifetime of pieces has been dramatically increased. There are different methods for making above-mentioned nano-structured coating, such as plasma aerosol, chemical deposition, and electrophoretic. It seems that electrophoretic coating method has higher compatibilities for different applications.

### 6.10.4 Using Nanocomposite Coating for Food Packaging

The food is offered in different packages, in terms of the food kind and required time. In some food the product should maintain its original and natural shape. One of important points in this field is paying attention on purchasers needs. Consumer is interested to buy fresh food with least of necessary changes during extra processes for increase of food preservation. Since its initiation time, food packaging industry has been subjected to many changes, based on demands of consumers, such as improvement of preservation, food health, and food compatibility with environment. Responding to these needs, there have been various researches in field of packaging quality and use of new intelligent materials.

Todays, technological achievements in food packaging industry have enabled us to apply intelligent packaging in order to change conditions and data delivery from food situation. This package is called active packaging. One applied method, is use of nano-composite coating to coat plastic layers. Over the time, food releases gasses and moisture in their packages. In some packaging gas and moisture absorbent are used, which leads to healthiness and preservation of the food. Some intelligent coatings show leakage or increase of temperature. Nowadays, there are some attempts to promote packaging quality through coating of food packages using anti-microbial coatings. Till now, use of these coatings has not been of much interest. Regarding available technologies use of these coatings is not economic yet. However, some active companies in this field hope to produces low cost surfaces with decent anti-bacterial property—using nano-coating technology—to coat food products. Another application of nano-coating is production of biosensors, attached to packages in coating form. Biosensors can offer information about quality of packaged materials, their state of healthiness, and etc. [85–91]

### *6.10.5 Antipollution Materials in Shipping Industry*

Recently, nano-materials are used in shipping industry as an antipollution and deodorant agent. Nano-particles are remained in network of antipollution coating and release their ions over the time, which causes antipollution traits. Todays, use of Sn-tributyl, once broadly used, is stopped and there is a need for other substitute materials. Lifetime of materials such as copper oxide and other similar materials is not efficient for this application, though nano-materials used for this application seems to be suitable. Polluted Copper oxide or zinc oxide nano-particles can be efficiently replaced at coating formulation of shipping industry. Researchers have shown that these materials exhibit a loner lifetime for antimicrobial applications.

### *6.10.6 Nano-Coating Use Against SARS Virus*

Recently, SARS virus is proposed as one of main dangers and there have been so many concerns about its epidemic issue. To deal with this virus, researchers of nano-material field have achieved nano-coating, which is a good weapon to stop this virus activity. These nano-materials include titanium oxide coated with Ag nano-particles. Researches have shown that release of Ag ions during a long time to stop activities of these viruses. These coatings with inappropriate ratio of constituents can cause serious damages to human body. There are some other researches performed by TN Nanovation. GmbH, which produce a nano-powder, called Nanozid, which is added as additive to the color, in order to coat diurnal appliances and tools such as beds and other staffs used in hospitals. These coatings, as well as the similar ones, can be used in food beverage industry.

### 6.10.7 Application of Ag Nanoparticles as Antibacterial Coating

German researchers at Institute for New Materials (INM) have created antibacterial surfaces with Ag nanoparticles. Adding a little amount of these materials to coating make it possible to obtain a big deal of these nano-materials. These materials can release a considerable deal of Ag ions, which is also able to eliminate other pollutions. Different nano-coatings for antipollution goals are available in the market; however produced compound in this research institute is of a unique application variety. The coating can be applied in all surfaces which can potentially be harmful for health. Among these materials one can name hospitals, offices, public places and even houses. These coatings are used on all touchable surfaces, even metallic, plastic, or glass ones. They can also be useful in appliances with public uses [92–100].

### 6.10.8 Using $TiO_2$ Nano-Particles to Decrease Environmental Contaminations

Contaminated materials, especially those caused by oil pollutions, due to transportation process or other similar accidents are among most important sources for environmental contaminations. Another case of pollution is one induced by uncontrolled release of industrial wastewater. There are different methods to decrease pollutions caused by organic materials, e.g. using catalysts for degradation of organic molecules to harmless ones. Among most important catalysts one can name $TiO_2$ particles. These particles are coated on efficient substrates and exposed to ultraviolet light in particular pools. Energy gap of this semi-conductor is about 3 eV. Due to radiation of ultraviolet light, there develops an oxidizing property in electron, produced cavity, and the material. Due to oxidization, they are degraded to some harmless materials, such as $H_2O$, $CO_2$, and other inorganic materials. Some experiments suggest that a wastewater polluted with oil organic materials can be completely degraded after 7 days. To improve efficiency of these nano-particles there also is a use of $TiO_2$ polluted with Fe and Er. Due to pollution energy gap significantly decreases and oxidization process happens under radiation with longer wavelength.

## 6.11 Electrical and Electronic Applications

### 6.11.1 Production of Transparent Conductor Coatings by Carbon Nano-Tubes

With respect to broad applications of transparent conductor coatings there have been developed different materials and methods to produce these coatings.

Among most commonplace methods one can name using ITO coatings. Regarding achievements in nano-technology, another method is application of carbonic nano-particles and nano-tubes. In case of broad using these materials for transparent conductor coating, there would be a dramatic growth in application of these coatings. One of famous companies in this field is Eikos which uses carbon nano-tubes to product conductor coatings. For industrial applications, produced layers must be of high transparency, suitable conductivity, low price, decent printability, and flexibility and resistance against environmental agents. Carbon nano-tubes have efficient electrical and thermal conductivity, equal to those of diamonds. Regarding their low weights (1/6 of steel's) this tubes have considerable hardness. Todays, vaporization of polluted zinc oxide with $InSnO_2$ in vacuum tube is applied as a standard industrial coating. The thin film of this material has efficient light transparency and excellent conductivity. Thin films of ITO are not suitable to coat polymeric surfaces; also conductivity of pieces considerably decreases through its bending and other types of deformation.

Metallic nano-particles have fairly high price and very low transparency and then are not convenient for painting. According to mentioned points produced transparence conductive coating with carbon nano-tubes is completely efficient, compared with the other mentioned methods. They only setback of this method is its lower, but enough, conductivity. For different coatings, depending on type and application of the coating, different materials are used. Among these materials one can mention atomic nano-clusters such as quantum particles, inorganic and molecular particles, nano-tubes with quantum wires, and nano-composites. The other important used compounds for coating are:

- Silicide, carbide, nitride, and oxide
- Boride, selenaride, fluoride, and various types of sulfides
- Halide, alloys, intermetallic materials, metals
- And organic polymers

### *6.11.2 Application of Nano-Coating on Solar Cells*

Since nano-coating can be applied to improve quality of existed products and produce of new materials, some companies, e.g. Nanogate have used these coatings to promote available systems. This company, which has previously developed sport facilities with nano-coating, attempts to improve some of its other products. One of its study fields is antipollution coating of solar cells. Coatings surface of solar cells with antipollution and snow resistant coatings, a bigger deal of solar energy can be absorbed and solar cells show a significant efficiency [101–107].

### 6.11.3 Nano-Coating of Nickel Particles by Oxides

Ceramic multilayer capacitor is a piece with broad use in electronic. Using these capacitors in smaller volumes and materials such as $BaTiO_3$, it is possible to achieve higher capacities. For economizing these capacitors there was an effort to alternate Pd/Ag electrodes with those made of metals such as Ni. These particles problem is their oxidation with increase of temperature, happening in concentrated circuits with many capacitors. One solution for this phenomenon is using oxide coating with stable oxides. $BaTiO_3$ is rather desirable for this goal. Unless coating with this material is performed in nano thickness, it is probable dielectric properties of the layer be changes. For this aim, method of TiCl hydrolyzing in butanone is applied. Using this method it is predicted to obtain low price high efficiency capacitor in small volumes.

### 6.11.4 Using Polarizer Nano-Layers to Produce LCD Monitors

Todays, a big share of monitors is devoted to LCDs. For their many advantages, compared with CRT monitors, their application is dramatically increase. These monitors include two groups: Active Matrix and Passive Matrix monitors. About 30% of monitors' price is for their polarizer part. Nowadays, a type of 200 μm layers is used to produce Active LCDs. Optiva Company is determined to use self-organizer nano-structures which are capable of being coated with (Thin Crystal Film) TCF method. These layers should be of equal cohesion and homogeneity in any surface. In case of using this method there will be monitors with high resolution, broader sight angle, and lower prices.

### 6.11.5 Produce of Electrically Conductive Transparence Nano-Coatings

Eikos and FLEXcom Companies are determined to cooperatively produce electrically conductive transparence layers with carbon nano-tubes. Defense Ministry of the United State has devoted 1 million dollars to development of this technology. The layers can be used in solar cells, flat monitors, organic photonic diodes, intelligent windows, and etc. Compared with traditional ITO (Indium Tin Oxide) methods, this technology is cheaper and more trustable, with less volume and higher efficiency. Regarding present applications for ITO it seems there will be a good market for this new product.

### 6.11.6 *Increase of Data Storing Capacity with Magnetic Nano-Layers*

Thanks to nano-layers, researchers have achieved higher density of storing in thin layers. In this method thin magnetic contained nano-layers are used and storing capacity has reached to 12 Gb/in$^2$; however the bigger figures are also achievable. Researchers believe that the nano-particle contained layers, as well as having an enhancement in their efficiency and homogeneity, will completely dominate present products.

## 6.12 Lubricating and the Other Applications

Using nano-technology and Self-Organizing polymers and nano-particles, Nanogate Coating Systems Gmbh has achieved production of very high quality oils for sport applications such as ski. Using this lubricators is easier that previous ones; also they are more compatible with variant climates and increase speed and maneuverability in slopes. The layers are also compatible with different types of snow.

## 6.13 Ag-Polluted $SnO_2$ Particles

Recently, Nanophute Technology group announced produce of Ag-polluted $SnO_2$ particles. These nano-particles diameter is about 30 nm and contain 3 weight percent of Ag. The nanoparticles are currently used in semi-industrial scale. Ag-polluted $SnO_2$ nano-particles are used for many aims such as industrial anti-microbial applications of wood protection, additives for plastic, and for electrically conductive coating.

## 6.14 Development of Nano-Coating for Surface Lubrication

Nano-coated surfaces have shown an acceptable potential for lubrication. For this aim, nano-metric coating of materials such as $Al_2O_3/TiO_2$, WC/Co, and $Cr_2O_3/TiO_2$ have been widely focused. Another applied material is Yttria-stablized-Zinconia. Today, many companies and institutes dependent to nano-particles coating and production, decided to apply available technologies for nano-coating. For example, one of widely used methods in coating industry is thermal spray. Use of this method for nano-coating is accompanied with some difficulties. It has been tried to eliminate the problems. Defense centers such as Navy Force of United States have extensively invested in this field of nano-coating research and

development. For this aim there is a comprehensive cooperation between academic and industrial centers [108–121].

## 6.15 Size Dependency in Nanocomposite Layers

Hard silica/epoxy nanocomposite layers were prepared by spinning method on the surface of AA6082 aluminum alloy with addition of CdTe quantum dots as the second phase in hard nanocomposite coating with different ratios in respect to main phase (silica nanoparticulates). Electrical conductivity tests have been done on the coatings for investigation of the possible enhanced or inverse effects of addition QDs on properties of hard nanocomposite. The effects of some effective factors have been investigated and it has been shown that by adding QD nanoparticulates the electrical conductivity of layers is completely controllable without adverse effect on wear resistance. Figure 6.15 shows the effect of different rotating speeds on the electrical conductivity of obtained layers. Density of different nanoparticulates will decrease significantly by increasing rotating speed. By increasing rotating speed, nanoparticulates will distribute far from each other. By increasing rotating speed, electrical resistivity completely obey a linear relation with respect to rotating speed.

Electrical resistivity acts to some what different from previous relations however it remains also completely predictable. Its plot (Fig. 6.16) can be divided into three sections. First section is a completely slight linear increase follows by a severe linear increase in second section and the third section is like the first one. It is worthwhile mentioning here that due to difference in trends which observed in this plot these sets of experiments have been done three times and reproducibility of the results has been proved. It can be said that due to the effective share of QD nanoparticulates in electrical conductivity of obtained layers, the amount of them and bridging among them will cause the rapid increase in second section of the curve. After reaching a special level for presence of QD nanoparticulates and increasing their joining, the electrical conductivity will increase again with a slight slope, as it can be seen in third section of the curve.

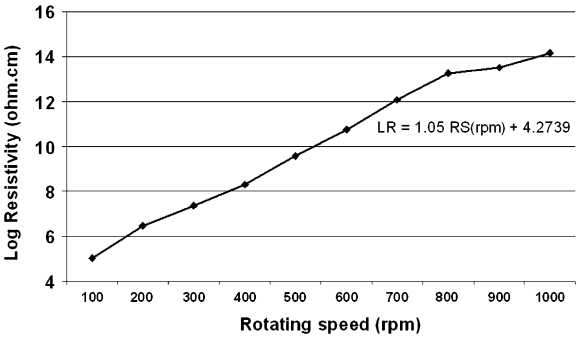


**Fig. 6.15** Effect of rotating speed on electrical resistivity of different silica/epoxy nanocomposite layers [122]

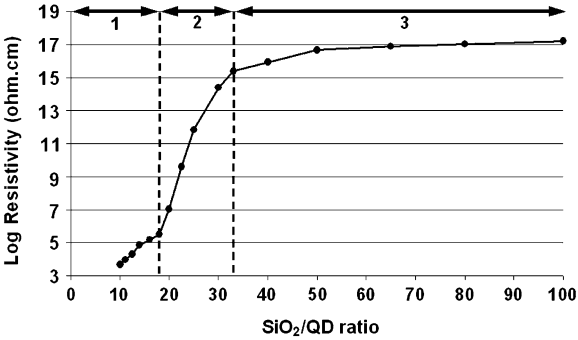


**Fig. 6.16** Effect of $SiO_2$/QD ratio on electrical resistivity of different obtained layers [122]

## References


1. Feng, J.L., Yue, C.Y., Chian, K.S.: Development and characterization of bismaleimides containing aliphatic chain for microelectronics application. E-Polymers 1–11 (2006)
2. Goodman, J.: Microelectronics lessons apply to fuel cell development. Fuel Cells Bull. **2003**, 10–12 (2003)
3. Kang, S.K.: Development of lead (Pb)-free interconnection materials for microelectronics. Metals Mater. Int. **5**, 545–549 (1999)
4. Siemroth, P., Schülke, T.: Copper metallization in microelectronics using filtered vacuum arc deposition—principles and technological development. Surf. Coat. Technol. **133–134**, 106–113 (2000)
5. Symko, O.G., Abdel-Rahman, E., Kwon, Y.S., Emmi, M., Behunin, R.: Design and development of high-frequency thermoacoustic engines for thermal management in microelectronics. Microelectron. J. **35**, 185–191 (2004)
6. Zhang, H.Y., Pinjala, D., Joshi, Y.K., Wong, T.N., Toh, K.C.: Development and characterization of thermal enhancement structures for single-phase liquid cooling in microelectronics systems. Heat Transf. Eng. **28**, 997–1007 (2007)
7. Lakatos, A., Erdelyi, G., Langer, G.A., Daroczi, L., Vad, K., Csik, A., Dudas, A., Beke, D.L.: Investigations of diffusion kinetics in Si/Ta/Cu/W and Si/Co/Ta systems by secondary neutral mass spectrometry. Vacuum **84**, 953–957 (2010)
8. Cojocaru-Mirédin, O., Perrin-Pellegrino, C., Mangelinck, D., Blavette, D.: Boron redistribution during reactive diffusion in Ni-Si contacts. Microelectron. Eng. **87**, 271–273 (2010)
9. Tam, P.L., Jelvestam, U., Nyborg, L.: Corrosion behaviour of amorphous Ni-Si thin films on AISI 304L stainless steel. Mater. High Temp. **26**, 177–186 (2009)
10. Schaefer, A., Zielasek, V., Schmidt, T., Sandell, A., Schowalter, M., Seifarth, O., Walle, L.E., Schulz, C., Wollschäger, J., Schroeder, T., Rosenauer, A., Falta, J., Bäumer, M.: Growth of praseodymium oxide on Si(111) under oxygen-deficient conditions. Phys. Rev. B. Condensed Matter Mater. Phys. **80**, 045414-0-13 (2009)
11. Cojocaru-Mirēdin, O., Cadel, E., Blavette, D., Mangelinck, D., Hoummada, K., Genevois, C., Deconihout, B.: Atomic-scale redistribution of Pt during reactive diffusion in Ni (5% Pt)-Si contacts. Ultramicroscopy **109**, 797–801 (2009)
12. Chirkin, A.D., Lavrenko, V.O., Talash, V.M.: High-temperature and electrochemical oxidation of transition metal silicides. Powder Metall. Metal Ceram. **48**, 330–345 (2009)
13. Hähnel, A., Pippel, E., Woltersdorf, J.: Control of Ni/SiC reactions by germanium, studied on the atomic scale. Scripta Mater. **60**, 858–861 (2009)
14. Agarwal, G., Sharma, P., Jain, A., Lal, C., Kabiraj, D., Jain, I.P.: Ion beam induced mixing at Co/Si interface. Vacuum **83**, 397–400 (2008)

15. Ohno, T., Numakura, K., Itoh, H., Suzuki, H., Matsuda, T.: Control of the quantum size effect of $TiO_2$-$SiO_2$ hybrid particles. Mater. Lett. **63**, 1737–1739 (2009)
16. Chu, M.M., Chou, J.H.: Advances in selective wet etching for nanoscale NiPt salicide fabrication. Jpn. J. Appl. Phys. **49**, 06GG161–06GG165 (2010)
17. Ghai, D., Mohanty, S.P., Kougianos, E.: A variability tolerant system-on-chip ready nano-CMOS analogue-to-digital converter. Int. J. Electron. **97**, 421–440 (2010)
18. Raoult, J., Pascal, F., Leyris, C.: I-V and low frequency noise characterization of poly and amorphous silicon Ti- and Co-salicide resistors. Thin Solid Films **518**, 2497–2500 (2010)
19. Guangxin, D., Lingdou, C., Zhongli, L.: Design for an IO block array in a tile-based FPGA. J. Semicond. **30**, 085008-1-6 (2009)
20. Zimmermann, S., Zhao, Q.T., Höhnemann, H., Wiemer, M., Kaufmann, C., Mantl, S., Dudek, V., Gessner, T.: Roughness improvement of the $CoSi_2$/Si-interface for an application as buried silicide. Microelectron. Eng. **84**, 2537–2541 (2007)
21. Hwang, K.J., Oh, J.H., Sung, N.K., Ryu, D.Y., Sa, S.H., Park, K.J., Lee, J.K., Lee, J.G., Park, S.H., Goo, T.G., Lee, H.D.: Characterization and improvement of reverse leakage current of shallow silicided junction for Sub-100 nm CMOS technology utilizing N2 PAI. J. Korean Phys. Soc. **49**, S795–S799 (2006)
22. Erbetta, D., Lazzari, C.M., Brambilla, M., Marangon, T.: Impact of an As implant before $CoSi_2$ formation on the sheet resistance and junction breakdown voltage. Microelectron. Eng. **83**, 2258–2263 (2006)
23. Zimmermann, S., Zhao, Q.T., Höhnemann, H., Wiemer, M., Kaufmann, C., Mantl, S., Dudek, V., Gessner, T.: Different approaches to integrate patterned buried $CoSi_2$ layers in SOI substrates. Microelectron. Eng. **83**, 2112–2116 (2006)
24. Tan, S.Y.: Dopant enhanced in nickel silicide formation for high-k dielectric applications. J. Mater. Sci. Mater. Electron. **21**, 1195–1201 (2010)
25. Li, Z., Gordon, R.G., Li, H., Shenai, D.V., Lavoie, C.: Formation of nickel silicide from direct-liquid-injection chemical-vapor-deposited nickel nitride films. J. Electrochem. Soc. **157**, H679–H683 (2010)
26. Chen, X., Zhao, A., Shao, Z., Li, C., Williams, C.T., Liang, C.: Synthesis and catalytic properties for phenylacetylene hydrogenation of silicide modified nickel catalysts. J. Phys. Chem. C **114**, 16525–16533 (2010)
27. Verleysen, E., Bender, H., Richard, O., Schryvers, D., Vandervorst, W.: Characterization of nickel silicides using EELS-based methods. J. Microsc. **240**, 75–82 (2010)
28. Vassilevski, K., Nikitina, I.P., Horsfall, A.B., Wright, N.G., Johnson, C.M.: Growth of few layers graphene on silicon carbide from nickel silicide supersaturated with carbon. In: Materials Science Forum, p. 589. (2010)
29. Vassilevski, K., Nikitina, I.P., Horsfall, A.B., Wright, N.G., Johnson, C.M.: 6 kV, 10.5 mOhm $cm^2$ nickel silicide Schottky diodes on commercial 4H-SiC epitaxial wafers. In: Materials Science Forum, pp. 897–900. (2010)
30. Bhaskaran, M., Sriram, S., Holland, A.S.: Interfacial resistive properties of nickel silicide thin films to doped silicon. J. Electrochem. Soc. **157**, H842–H846 (2010)
31. Chen, H.Y., Lin, C.Y., Huang, C.C., Chien, C.H.: The effect of pulsed laser annealing on the nickel silicide formation. Microelectron. Eng. **87**, 2540–2543 (2010)
32. Kobayashi, K., Watanabe, H., Maekawa, K., Kashihara, K., Yamaguchi, T., Asai, K., Hirose, Y.: Oxygen distribution in nickel silicide films analyzed by time-of-flight secondary ion mass spectrometry. Micron **41**, 412–415 (2010)
33. Song, O., Kim, K., Choi, Y.: Nano-thick nickel silicide and polycrystalline silicon on glass substrate with low temperature catalytic CVD. J. Korean Inst. Metals Mater. **48**, 660–666 (2010)
34. Utlu, G., Artunç, N., Budak, S., Tari, S.: Structural and electrical characterization of the nickel silicide films formed at 850°C by rapid thermal annealing of the Ni/Si(1 0 0) films. Appl. Surf. Sci. **256**, 5069–5075 (2010)

35. De Keyser, K., Van Bockstael, C., Van Meirhaeghe, R.L., Detavernier, C., Verleysen, E., Bender, H., Vandervorst, W., Jordan-Sweet, J., Lavoie, C.: Phase formation and thermal stability of ultrathin nickel-silicides on Si(100). Appl. Phys. Lett. **96**, 173503-1-3 (2010)
36. Verleysen, E., Bender, H., Schryvers, D., Vandervorst, W.: Chemical analysis of nickel silicides with high spatial resolution by combined EDS, EELS and ELNES. J. Phys.: Conf. Series **209**, 1–4 (2010)
37. Tsui, B.Y., Lee, C.M.: Thermal stability of nickel silicide and shallow junction electrical characteristics with carbon ion implantation. Jpn. J. Appl. Phys. **49**, 04DA04-1-6 (2010)
38. Tan, O.K., Zhu, W., Yan, Q., Kong, L.B.: Size effect and gas sensing characteristics of nanocrystalline $xSnO_2$-$(1-x)\alpha$-$Fe_2O_3$ ethanol sensors. Sens. Actuators B Chem. **65**, 361–365 (2000)
39. Yoon, J.H.: Synthesis and charge storage properties of double-layered NiSi nanocrystals. J. Nanopart. Res. **12**, 2387–2391 (2010)
40. Yoo, J.H., Sohn, H., Ko, D.H., Cho, M.H.: Enhancement of thermal stability in Ni silicides on Epi-$Si_{1-x}$ $C_x$ by Pt addition. J. Electrochem. Soc. **157**, H837–H841 (2010)
41. Lee, S.W., Huang, S.H., Cheng, S.L., Chen, P.S., Wu, W.W.: Ni silicide formation on epitaxial $Si_{1-Y}C_y$/(001) layers. Thin Solid Films **518**, 7394–7397 (2010)
42. Alptekin, E., Ozturk, M.C.: $Ni_xPt_{1-x}Si$/n-Si contacts with sub-0.1 eV effective Schottky barrier heights obtained by sulfur segregation. Microelectron. Eng. **87**, 2358–2360 (2010)
43. Whang, S.J., Joo, M.S., Seo, B.M., Chang, K.E., Kim, W.K., Jung, T.W., Kim, G.H., Lim, J.Y., Kim, K.Y., Hong, K., Park, S.K.: Thermally stable NiSi gate electrode with TiN barrier metal for high-density NAND flash memory devices. Jpn. J. Appl. Phys. **49**, 04DA17-1-4 (2010)
44. Imbert, B., Pantel, R., Zoll, S., Gregoire, M., Beneyton, R., Medico, S.D., Thomas, O.: Nickel silicide encroachment formation and characterization. Microelectron. Eng. **87**, 245–248 (2010)
45. Lee, S.W., Huang, S.S., Hsu, H.C., Nieh, C.W., Tsai, W.C., Lo, C.P., Lai, C.H., Tsai, P.Y., Wang, M.Y., Wu, C.M., Lei, M.D.: C redistribution during Ni silicide formation on $Si_{1-y}$ $C_y$ epitaxial layers. J. Electrochem. Soc. **157**, H297–H300 (2010)
46. Lee, J.B., Jeong, S.Y., Park, B.J., Choi, C.J., Hong, K., Whang, S.J., Seong, T.Y.: Improved electrical and thermal properties of nickel silicides by using a NiCo interlayer. Superlattices Microstruct. **47**, 259–265 (2010)
47. Tsui, B.Y., Hsieh, C.M., Hung, Y.R., Yang, Y., Shen, R., Cheng, S., Lin, T.: Improvement of the thermal stability of NiSi by germanium Ion implantation. J. Electrochem. Soc. **157**, H137–H143 (2010)
48. Wang, C.C., Lin, H.H., Chen, M.C.: Thermal stability of Cu/NiSi-contacted p+n shallow junction. Jpn. J. Appl. Phys., Part 1: Regular Papers and Short Notes and Review Papers **43**, 5997–6000 (2004)
49. Wang, R.N., He, Y., Feng, J.Y.: Explanation of the enhancement of NiSi thermal stability according to TFD equations and Miedema's model. Nucl. Instrum. Methods Phys. Res. Sect. B Beam Interact. Mater. Atoms **222**, 462–468 (2004)
50. Zhao, F.F., Zheng, J.Z., Shen, Z.X., Osipowicz, T., Gao, W.Z., Chan, L.H.: Thermal stability study of NiSi and $NiSi_2$ thin films. Microelectron. Eng. **71**, 104–111 (2004)
51. Wang, R.N., Feng, J.Y.: Comparison of the thermal stabilities of NiSi films in Ni/Si, Ni/Pd/Si and Ni/Pt/Si systems. J. Phys. Condensed Matter **15**, 1935–1942 (2003)
52. Wang, R.N., Feng, J.Y., Huang, Y.: Mechanism about improvement of NiSi thermal stability for Ni/Pt/Si(1 1 1) bi-layered system. Appl. Surf. Sci. **207**, 139–143 (2003)
53. Wong, A.S.W., Chi, D.Z., Loomans, M., Ma, D., Lai, M.Y., Tjiu, W.C., Chua, S.J., Lim, C.W., Greene, J.E.: F-enhanced morphological and thermal stability of NiSi films on $BF_+^{2-}$ implanted Si(001). Appl. Phys. Lett. **81**, 5138–5140 (2002)
54. Liu, J.F., Feng, J.Y., Zhu, J.: Comparison of the thermal stability of NiSi films in Ni/Pt/(111)Si and Ni/Pt/(100)Si systems. J. Appl. Phys. **90**, 745–749 (2001)
55. Liu, J.F., Chen, H.B., Feng, J.Y.: Enhanced thermal stability of NiSi films on Si(1 1 1) substrates by a thin Pt interlayer. J. Cryst. Growth **220**, 488–493 (2000)

56. Liu, J.F., Chen, H.B., Feng, J.Y., Zhu, J.: Improvement of the thermal stability of NiSi films by using a thin Pt interlayer. Appl. Phys. Lett. **77**, 2177–2179 (2000)
57. Mangelinck, D., Dai, J.Y., Pan, J.S., Lahiri, S.K.: Enhancement of thermal stability of NiSi films on (100)Si and (111)Si by Pt addition. Appl. Phys. Lett. **75**, 1736–1738 (1999)
58. Kale, R.B., Lokhande, C.D.: Influence of air annealing on the structural, optical and electrical properties of chemically deposited CdSe nano-crystallites. Appl. Surf. Sci. **223**, 343–351 (2004)
59. Du, H., Lee, S.W., Gong, J., Sun, C., Wen, L.S.: Size effect of nano-copper films on complex optical constant and permittivity in infrared region. Mater. Lett. **58**, 1117–1120 (2004)
60. Tang, Z.K., Kawasaki, M., Ohtomo, A., Koinuma, H., Segawa, Y.: Self-assembled ZnO nano-crystals and exciton lasing at room temperature. J. Cryst. Growth **287**, 169–179 (2006)
61. Bilotsky, Y., Tomchuk, P.M.: Peculiarity of electron-phonon energy exchange in metal nanoparticles and thin films. Surf. Sci. **602**, 383–390 (2008)
62. Grandusky, J.R., Gibb, S.R., Mendrick, M.C., Schowalter, L.J.: Properties of mid-ultraviolet light emitting diodes fabricated from pseudomorphic layers on bulk aluminum nitride substrates. Appl. Phys. Express **3**, 072103-1-3 (2010)
63. Hirayama, H., Tsukada, Y., Maeda, T., Kamata, N.: Marked enhancement in the efficiency of deep-ultraviolet AlGaN light-emitting diodes by using a multiquantum-barrier electron blocking layer. Appl. Phys. Express **3**, 031002-1-3 (2010)
64. Lee, K.B., Parbrook, P.J., Wang, T., Bai, J., Ranalli, F., Airey, R.J., Hill, G.: Effect of the AlGaN electron blocking layer thickness on the performance of AlGaN-based ultraviolet light-emitting diodes. J. Cryst. Growth **311**, 2857–2859 (2009)
65. Takeuchi, M., Maegawa, T., Shimizu, H., Ooishi, S., Ohtsuka, T., Aoyagi, Y.: AlN/AlGaN short-period superlattice sacrificial layers in laser lift-off for vertical-type AlGaN-based deep ultraviolet light emitting diodes. Appl. Phys. Lett. **94**, 061117-1-3 (2009)
66. An, S.J., Yi, G.C.: Near ultraviolet light emitting diode composed of n-GaN/ZnO coaxial nanorod heterostructures on a p-GaN layer. Appl. Phys. Lett. **91**, 123109-1-3 (2007)
67. Huang, G.S., Kuo, H.C., Lo, M.H., Lu, T.C., Tsai, J.Y., Wang, S.C.: Improvement of efficiency and ESD characteristics of ultraviolet light-emitting diodes by inserting AlGaN and SiN buffer layers. J. Cryst. Growth **305**, 55–58 (2007)
68. Georgieva, J., Armyanov, S., Valova, E., Poulios, I., Sotiropoulos, S.: Enhanced photocatalytic activity of electrosynthesised tungsten trioxide-titanium dioxide bi-layer coatings under ultraviolet and visible light illumination. Electrochem. Commun. **9**, 365–370 (2007)
69. Ichikawa, M., Kobayashi, K., Koyama, T., Taniguchi, Y.: Intense and efficient ultraviolet electroluminescence from organic light-emitting devices with fluorinated copper phthalocyanine as hole injection layer. Thin Solid Films **515**, 3932–3935 (2007)
70. Sakai, N., Prasad, G.K., Ebina, Y., Takada, K., Sasaki, T.: Layer-by-layer assembled $TiO_2$ nanoparticle/PEDOT-PSS composite films for switching of electric conductivity in response to ultraviolet and visible light. Chem. Mater. **18**, 3596–3598 (2006)
71. Kyono, T., Hirayama, H., Akita, K., Nakamura, T., Adachi, M., Ando, K.: Influence of residual oxygen impurity in quaternary InAlGaN multiple-quantum-well active layers on emission efficiency of ultraviolet light-emitting diodes on GaN substrates. J. Appl. Phys. **99**, 114509-1-7 (2006)
72. Izaki, M., Shinagawa, T., Takahashi, H.: Room temperature ultraviolet light emitting ZnO layer prepared by low-temperature electrodeposition. J. Phys. D Appl. Phys. **39**, 1481–1484 (2006)
73. Kwon, M.K., Park, I.K., Baek, S.H., Kim, J.Y., Park, S.J.: Si delta doping in a GaN barrier layer of InGaN/GaN multiquantum well for an efficient ultraviolet light-emitting diode. J. Appl. Phys. **97**, 1–3 (2005)
74. Liu, Y.H., Li, H.D., Ao, J.P., Lee, Y.B., Wang, T., Sakai, S.: Influence of undoped GaN layer thickness to the performance of AlGaN/GaN-based ultraviolet light-emitting diodes. J. Cryst. Growth **268**, 30–34 (2004)

75. Bu, I.Y.Y., Oei, S.P.: Hydrophobic vertically aligned carbon nanotubes on Corning glass for self cleaning applications. Appl. Surf. Sci. **256**, 6699–6704 (2010)
76. Katsumata, K., Okazaki, S., Cordonier, C.E., Shichi, T., Sasaki, T., Fujishima, A.: Preparation and characterization of self-cleaning glass for vehicle with niobia nanosheets. ACS Appl. Mater. Interfaces **2**, 1236–1241 (2010)
77. Peruchon, L., Puzenat, E., Herrmann, J.M., Guillard, C.: Photocatalytic efficiencies of self-cleaning glasses. Influence of physical factors. Photochem. Photobio. Sci. **8**, 1040–1046 (2009)
78. Kasanen, J., Suvanto, M., Pakkanen, T.T.: Self-cleaning, titanium dioxide based, multilayer coating fabricated on polymer and glass surfaces. J. Appl. Polym. Sci. **111**, 2597–2606 (2009)
79. Medina-Valtierra, J., Frausto-Reyes, C., Ramirez-Ortiz, J., Camarillo-Martínez, G.: Self-cleaning test of doped $TiO_2$-coated glass plates under solar exposure. Ind. Eng. Chem. Res. **48**, 598–606 (2009)
80. Peruchon, L., Puzenat, E., Girard-Egrot, A., Blum, L., Herrmann, J.M., Guillard, C.: Characterization of self-cleaning glasses using Langmuir-Blodgett technique to control thickness of stearic acid multilayers. Importance of spectral emission to define standard test. J. Photochem. Photobiol. A Chem. **197**, 170–176 (2008)
81. Zhao, X., Zhao, Q., Yu, J., Liu, B.: Development of multifunctional photoactive self-cleaning glasses. J. Non-Cryst. Solids **354**, 1424–1430 (2008)
82. Daiko, Y., Yajima, H., Kasuga, T.: Preparation of porous titanium phosphate glass-ceramics for $NH_3$ gas adsorption with self-cleaning ability. J. Eur. Ceram. Soc. **28**, 267–270 (2008)
83. Medina-Valtierra, J., Campos-Revna, S.J., Frausto-Reyes, C., Calixto, S., Ramírez-Ortíz, J.: Self-cleaning test of doped anatase-coated glass plates. Int. J. Chem. React. Eng. **5**, A101-1-4 (2007)
84. Mellott, N.P., Durucan, C., Pantano, C.G., Guglielmi, M.: Commercial and laboratory prepared titanium dioxide thin films for self-cleaning glasses: photocatalytic performance and chemical durability. Thin Solid Films **502**, 112–120 (2006)
85. Sanchez-Garcia, M.D., Hilliou, L., Lagaron, J.M.: Nanobiocomposites of Carrageenan, Zein, and Mica of interest in food packaging and coating applications. J. Agric. Food Chem. **58**, 6884–6894 (2010)
86. Azeredo, H.M.C., Mattoso, L.H.C., Avena-Bustillos, R.J., Filho, G.C., Munford, M.L., Wood, D., McHugh, T.H.: Nanocellulose reinforced chitosan composite films as affected by nanofiller loading and plasticizer content. J. Food Sci. **75**, N1–N7 (2010)
87. Jaworek, A.: Electrostatic micro- and nanoencapsulation and electroemulsification: a brief review. J. Microencapsul. **25**, 443–468 (2008)
88. Kuo, Y.C., Lee, J.W., Wang, C.J., Chang, Y.J.: The effect of Cu content on the microstructures, mechanical and antibacterial properties of Cr-Cu-N nanocomposite coatings deposited by pulsed DC reactive magnetron sputtering. Surf. Coat. Technol. **202**, 854–860 (2007)
89. Arshak, K., Adley, C., Moore, E., Cunniffe, C., Campion, M., Harris, J.: Characterisation of polymer nanocomposite sensors for quantification of bacterial cultures. Sens. Actuators B Chem. **126**, 226–231 (2007)
90. Avella, M., Bruno, G., Errico, M.E., Gentile, G., Piciocchi, N., Sorrentino, A., Volpe, M.G.: Innovative packaging for minimally processed fruits. Packag. Technol. Sci. **20**, 325–335 (2007)
91. Brody, A.L.: Food packaging technology. Food Technol. **57**, 52–54 (2003)
92. Cao, X., Tang, M., Liu, F., Nie, Y., Zhao, C.: Immobilization of silver nanoparticles onto sulfonated polyethersulfone membranes as antibacterial materials. Colloids Surf. B Biointerfaces **81**, 555–562 (2010)
93. Seo, Y.I., Hong, K.H., Kim, D.G., Kim, Y.D.: $Ag/Al(OH)_3$ mesoporous nanocomposite film as antibacterial agent. Colloids Surf. B Biointerfaces **81**, 369–373 (2010)

94. Dastjerdi, R., Montazer, M., Shahsavan, S.: A novel technique for producing durable multifunctional textiles using nanocomposite coating. Colloids Surf. B Biointerfaces **81**, 32–41 (2010)
95. Kim, S., Chung, H., Kwon, J.H., Yoon, H.G., Kim, W.: Facile synthesis of silver chloride nanocubes and their derivatives. Bull. Korean Chem. Soc. **31**, 2918–2922 (2010)
96. Moazami, A., Montazer, M., Rashidi, A., Rahimi, M.K.: Antibacterial properties of raw and degummed silk with nanosilver in various conditions. J. Appl. Polym. Sci. **118**, 253–258 (2010)
97. Pallavicini, P., Taglietti, A., Dacarro, G., Antonio Diaz-Fernandez, Y., Galli, M., Grisoli, P., Patrini, M., Santucci De Magistris, G., Zanoni, R.: Self-assembled monolayers of silver nanoparticles firmly grafted on glass surfaces: low $Ag^+$ release for an efficient antibacterial activity. J. Colloid Interface Sci. **350**, 110–116 (2010)
98. Lin, W.C., Chen, C.N., Tseng, T.T., Wei, M.H., Hsieh, J.H., Tseng, W.J.: Micellar layer-by-layer synthesis of $TiO_2$/Ag hybrid particles for bactericidal and photocatalytic activities. J. Eur. Ceram. Soc. **30**, 2849–2857 (2010)
99. Basri, H., Ismail, A.F., Aziz, M., Nagai, K., Matsuura, T., Abdullah, M.S., Ng, B.C.: Silver-filled polyethersulfone membranes for antibacterial applications—effect of PVP and TAP addition on silver dispersion. Desalination **261**, 264–271 (2010)
100. Jin, X., Li, M., Wang, J., Marambio-Jones, C., Peng, F., Huang, X., Damoiseaux, R., Hoek, E.M.V.: High-throughput screening of silver nanoparticle stability and bacterial inactivation in aquatic media: influence of specific ions. Environ. Sci. Technol. **44**, 7321–7328 (2010)
101. Hong, J.T., Seo, H., Lee, D.G., Jang, J.J., An, T.P., Kim, H.J.: A nano-porous $TiO_2$ thin film coating method for dye sensitized solar cells (DSSCs) using electrostatic spraying with dye solution. J. Electrost. **68**, 205–211 (2010)
102. Grinis, L., Kotlyar, S., Rühie, S., Grinblat, J., Zaban, A.: Conformal nano-sized inorganic coatings on mesoporous $TiO_2$ films for low-temperature dye-sensitized solar cell fabrication. Adv. Funct. Mater. **20**, 282–288 (2010)
103. Fan, S.Q., Li, C.J., Yang, G.J., Gao, J.C., Zhang, L.Z., Li, C.X., Wang, Y.Y.: Room-temperature deposition of nano-$TiO_2$ coating by vacuum cold spraying using $TiCl_4$-agglomerated nano-$TiO_2$ powder for flexible dye-sensitized solar cell. In: Key Engineering Materials, pp. 742–745. (2008)
104. Fan, S.Q., Li, C.J., Yang, G.J., Zhang, L.Z., Gao, J.C., Xi, Y.X.: Fabrication of nano-$TiO_2$ coating for dye-sensitized solar cell by vacuum cold spraying at room temperature. J. Therm. Spray Tech. **16**, 893–897 (2007)
105. Fan, S.Q., Li, C.J., Li, C.X., Liu, G.J., Yang, G.J., Zhang, L.Z.: Preliminary study of performance of dye-sensitized solar cell of nano-$TiO_2$ coating deposited by vacuum cold spraying. Mater. Trans. **47**, 1703–1709 (2006)
106. Von Sonntag, J., Getzmann, M., Braun, A., Mehnert, R.: Nano-composite synthesis with a TORUSMILL® for the scratch resistant coating of flexible solar cells [Nanokompositsynthese mit einer TORUSMILL® für die Kratz-festbeschichtung flexibler Solarzellen]. **38**, 16–17 (2005)
107. Nakato, K., Takabayashi, S., Imanishi, A., Murakoshi, K., Nakato, Y.: Stabilization of n-Si electrodes by surface alkylation and metal nano-dot coating for use in efficient photoelectrochemical solar cells. Sol. Energy Mater. Sol. Cells **83**, 323–330 (2004)
108. Liew, W.Y.H.: Low-speed milling of stainless steel with TiAlN single-layer and TiAlN/AlCrN nano-multilayer coated carbide tools under different lubrication conditions. Wear **269**, 617–631 (2010)
109. Zhang, Y.: A survey of boundary lubrication effect in elastohydrodynamic lubrication. J. Comput. Theor. Nanosci. **7**, 1496–1500 (2010)
110. Puértolas, J.A., Martíez-Nogués, V., Martíez-Morlanes, M.J., Mariscal, M.D., Medel, F.J., Ópez-Santos, C., Yubero, F.: Improved wear performance of ultra high molecular weight polyethylene coated with hydrogenated diamond like carbon. Wear **269**, 458–465 (2010)
111. Abdul Samad, M., Sinha, S.K.: Nanocomposite UHMWPE-CNT polymer coatings for boundary lubrication on aluminium substrates. Tribology Lett. **38**, 301–311 (2010)

112. Pham, D.C., Na, K., Yang, S., Kim, J., Yoon, E.S.: Nanotribological properties of silicon nano-pillars coated by a Z-DOL lubricating film. J. Mech. Sci. Technol. **24**, 59–65 (2010)
113. Koshy, R.A., Graham, M.E., Marks, L.D.: Temperature activated self-lubrication in CrN/$Mo_2N$ nanolayer coatings. Surf. Coat. Technol. **204**, 1359–1365 (2010)
114. Mulligan, C.P., Blanchet, T.A., Gall, D.: CrN-Ag nanocomposite coatings: tribology at room temperature and during a temperature ramp. Surf. Coat. Technol. **204**, 1388–1394 (2010)
115. Zhang, Q., Xiao, F., Guo, H., Li, C., Gao, L., Guo, X., Han, W., Bondarev, A.B.: Warm negative incremental forming of magnesium alloy AZ31 Sheet: new lubricating method. J. Mater. Process. Technol. **210**, 323–329 (2010)
116. Levashov, E.A., Zamulaeva, E.I., Pogozhev, Y.S., Kurbatkina, V.V.: Nanoparticle dispersion strengthened WC-C based coatings on Ti-alloy produced by sequential chemical reaction assisted pulsed electrospark deposition. Plasma Process. Polym. **6**, S102–S106 (2009)
117. Hope, P.: Developing an electrophoretically depositable self-lubricating nanocomposite paint process for a short recoil semi-automatic handgun application. In: Key Engineering Materials, pp. 157–163. (2009)
118. Bobzin, K., Bagcivan, N., Immich, P., Warnke, C., Klocke, F., Zeppenfeld, C., Mattfeld, P.: Advancement of a nanolaminated TiHfN/CrN PVD tool coating by a nano-structured CrN top layer in interaction with a biodegradable lubricant for green metal forming. Surf. Coat. Technol. **203**, 3184–3188 (2009)
119. Dasch, J.M., Ang, C.C., Wong, C.A., Waldo, R.A., Chester, D., Cheng, Y.T., Powell, B.R., Weiner, A.M., Konca, E.: The effect of free-machining elements on dry machining of B319 aluminum alloy. J. Mater. Process. Technol. **209**, 4638–4644 (2009)
120. Nie, C., Liu, X., Watanabe, H.: The lubrication properties of diamond-like carbon coatings in engine oil. In: Materials Science Forum, pp. 652–657. (2009)
121. Kang, J.J., Wang, C.B., Wang, H.D., Xu, B.S., Liu, J.J., Li, G.L.: Characterization and tribological properties of composite 3Cr13/FeS layer. Surf. Coat. Technol. **203**, 1927–1932 (2009)
122. Aliov, M.K., Sabur, A.R.: Formation of a novel hard binary $sio_2$/quantum dot nanocomposite with predictable electrical conductivity. Mod. Phys. Lett. B **24**, 89–96 (2010)